NOTE TO USERS

This reproduction is the best copy available.



THE OPTIMUM DESIGN OF EPICYCLIC TRAINS OF SPHERICAL CAM-ROLLER PAIRS

Sergio Hernandez

Department of Mechanical Engineering
McGill University, Montreal

June, 2004

A Thesis submitted to the Faculty of Graduate Studies and Research in partial fulfilment of the requirements for the degree of Master of Engineering

© S. HERNANDEZ, 2004



Library and Archives Canada

Bibliothèque et Archives Canada

Published Heritage Branch

Direction du Patrimoine de l'édition

395 Wellington Street Ottawa ON K1A 0N4 Canada 395, rue Wellington Ottawa ON K1A 0N4 Canada

> Your file Votre référence ISBN: 0-494-06555-9 Our file Notre référence ISBN: 0-494-06555-9

NOTICE:

The author has granted a nonexclusive license allowing Library and Archives Canada to reproduce, publish, archive, preserve, conserve, communicate to the public by telecommunication or on the Internet, loan, distribute and sell theses worldwide, for commercial or noncommercial purposes, in microform, paper, electronic and/or any other formats.

AVIS:

L'auteur a accordé une licence non exclusive permettant à la Bibliothèque et Archives Canada de reproduire, publier, archiver, sauvegarder, conserver, transmettre au public par télécommunication ou par l'Internet, prêter, distribuer et vendre des thèses partout dans le monde, à des fins commerciales ou autres, sur support microforme, papier, électronique et/ou autres formats.

The author retains copyright ownership and moral rights in this thesis. Neither the thesis nor substantial extracts from it may be printed or otherwise reproduced without the author's permission.

L'auteur conserve la propriété du droit d'auteur et des droits moraux qui protège cette thèse. Ni la thèse ni des extraits substantiels de celle-ci ne doivent être imprimés ou autrement reproduits sans son autorisation.

In compliance with the Canadian Privacy Act some supporting forms may have been removed from this thesis.

While these forms may be included in the document page count, their removal does not represent any loss of content from the thesis.

Conformément à la loi canadienne sur la protection de la vie privée, quelques formulaires secondaires ont été enlevés de cette thèse.

Bien que ces formulaires aient inclus dans la pagination, il n'y aura aucun contenu manquant.



ABSTRACT

Many a robotic pitch-roll wrist uses a bevel-gear differential train to drive the gripper. The innovative design of pitch-roll wrists using spherical cam-roller pairs is currently underway at McGill University's Centre for Intelligent Machines, with the aim of overcoming the drawbacks of bevel-gear trains. This innovative design relies on Speed-o-Cam, a new concept of speed-reduction mechanisms based on cams and pure-rolling contact, intended to replace gears and harmonic drives in applications where backlash, friction, and flexibility cannot be tolerated. The new mechanism consists mainly of a spherical conjugate cam subassembly and two roller-carrying disks.

We start with a study of cam curvature, with special focus on its machinability. Drawing from experience, we introduce the hypothesis that high curvature changes of a cam profile are at the source of the concentration of machining errors. As a consequence, the machining accuracy of the concave regions in a cam profile is substantially lower than that of its convex regions. To produce a more accurate cam we developed the geometric condition that guarantees a fully convex spherical cam profile.

The optimum design of the pitch-roll mechanism based on cam-roller pairs is reported here. The optimization is intended to simplify the subassembly of spherical conjugate cams of the old design by means of a layout of two pairs of spherical mechanisms of the Stephenson type and two conjugate cams mounted on distinct shafts. We focus on the optimum design of both the spherical cam-roller mechanism and the spherical Stephenson mechanism.

RÉSUMÉ

Plusieurs poignets robotiques effectuant des mouvements de tangage et de roulis utilisent un train differéntiel à engrenages coniques pour entraîner l'efecteur. Un concept innovateur de mécanisme tangage-roulis utilisant des paires de cames et roulis sphériques est en cours de mise au point à l'Université McGill, au Centre pour les Machines Intelligentes, avec le but de pallier aux inconvénients des trains à engrenages coniques. Cette conception novatrice est basée sur Speed-o-Cam, un nouveau mécanisme destiné à la réduction de vitesse, basé sur des ensembles cames-roulements, pour remplecer les réducteurs de vittesse classiques à engrenages ainsi que les harmonic drives, dans les applications ne tolérant pas le jeu, le frottement et la flexibilité. Ce nouveau mécanisme consiste essentiellement de sous-ensembles de cames sphériques conjugées et deux disques porteurs des roulements.

Nous commençons par étudier la courbure de la came, en mettant l'accent sur son usinage. Nous introduisons l'hypothèse selon lequelle les changements de courbure d'un profil de came sont à la source des concentration des erreurs d'usinage. Par conséquent, la précision de l'usinage des régions concaves d'un profil de came est notamment moins élevée que celle des régions convexes. Dans le but d'augmenter la précision des cames nous établissons une condition géométrique qui garantit un profil entièrement convexe de cames sphériques.

La conception optimale d'un mécanisme tangage-roulis basé sur des paires de cames et roulements est rapporté dans cette thèse. Le but de l'optimisation est de simplifier le sous-ensemble de cames sphériques conjuguées en adoptant une disposition de deux paires de mécanisme sphériques de type Stephenson et de deux cames conjugées montées sur des arbres indépendents. Nous faisons le point sur la conception optimale des mécanismes sphériques de type Stephenson et des cames-roulements.

ACKNOWLEDGEMENTS

I would like to thank my supervisor, *Professor Jorge Angeles*, for his support and encouragement in the work reported in this thesis. The guidance in profound knowledge and the feedback that he gave me with vigour and enthusiasm motivated me to improve my performance every day.

I am grateful to my parents and brothers and, specially, to the Sylvain-Hernández family for their constant encouragement and support, which gave me confidence during my studies.

I would like to thank: Khalid Al-Widyan, for his clarification of many concepts in my research area; Dr. Shaoping Bai, post-doctoral research associate in our group, for his help in the design of the cam-roller pair of the spherical pitch-roll wrist; Rija Ndrialisoa for his generous advice on the use of Pro/Engineer and Pro/Mechanica; and Danielle Nasrallah for helping me in translating the abstract into French.

I would also like to thank all my collegues and the staff of the Centre for Intelligent Machines (CIM) and the Department of Mechanical Engineering at McGill University, for their help, support, useful comments and making my stay at CIM a pleasant experience.

Finally, I would like to thank the most important of all, my *Lord Jesus*, for the encouragement that He gave me in the moments of weakness that I had during my studies.

The research work reported here was made possible by Strategic Grant STPGP 246488-01 of Canada's Natural Sciences and Engineering Research Council.

TABLE OF CONTENTS

ABSTRACT	j
RÉSUMÉ	ii
ACKNOWLEDGEMENTS	iii
LIST OF FIGURES	vi
LIST OF TABLES	viii
CHAPTER 1. Introduction	1
1.1. Background	1
1.2. Literature Review	4
1.3. Motivation	6
CHAPTER 2. The Synthesis of the Spherical Cam Mechanism	S
2.1. Spherical Cam Mechanisms	10
2.2. Curvature Analysis	12
2.3. Cam-Profile Determination	14
2.4. Convexity Condition	16
2.4.1. Concavity-Occurrence in the Cam Profile	17
CHAPTER 3. The Optimum Synthesis of a Spherical Stephenson Mechanism	21
3.1. The Spherical Stephenson Mechanism	22
3.2. Loop Equation	26
3.2.1. Rotation-Matrix Formulation	27
3.3. The Four-Bar Loop	28
3.4. The Five-Bar Loop	30
3.5. The IO Equation of the Spherical Stephenson Mechanism	34

TABLE OF CONTENTS

3.5.1. Elimination Procedure	35
3.6. Dimensional Synthesis of the Spherical Stephenson Mechanism	37
3.6.1. Spherical Drag-Link Mechanism	39
3.6.2. Optimum Synthesis of the Spherical Stephenson Mechanism	46
CHAPTER 4. Design Embodiment	52
4.1. Input-Output Relations	52
4.2. Transmission Angles	54
4.3. The Virtual Prototype	54
4.4. The Design of the Mechanism Mounting	59
CHAPTER 5. Concluding Remarks	65
5.1. Conclusions	65
5.2. Recommendations for Future Research	66
REFERENCES	68

LIST OF FIGURES

1.1	Wrist from a Remote-Control Manipulator (Rosheim, 1989)	2
1.2	Planar (a) and Spherical (b) Speed-o-Cam prototypes	2
1.3	Epicyclic mechanism based on cam-roller pairs	3
1.4	Hub with three conjugate cam subassemblies	6
1.5	Layout of the alternative mechanism	7
2.1	General layout of a spherical cam mechanism with a roller-follower	
	[taken from (González-Palacios and Angeles, 1993)]	10
2.2	An Indexing Cam Mechanism	11
2.3	Indexing mechanism with two conjugate cams 180° out of phase	12
2.4	Spherical radius of curvature	14
2.5	A sketch of the cam profile geometry	15
2.6	Synthesized concave cam (a) and its geodetic curvature (b)	19
2.7	Synthesized convex cam (a) and its geodetic curvature (b)	19
2.8	Convexity condition $F(\psi)$ vs. ψ : (a) for the concave cam; and (b)	
	for the convex cam	20
2.9	Convex cam profile	20
3.1	Spherical Stephenson mechanism	22
3.2	Double Cardan joint used in vehicles	24
3.3	The layout of the alternative mechanism separated in two chains	26
3.4	The four-bar loop	28
3.5	The five-bar loop	31

LIST OF FIGURES

3.6	The 4 bar mechanism	40
3.7	σ vs. δ for the main mechanism and its conjugate	46
3.8	The transmission angle μ vs δ	47
4.1	Output angles vs. ψ of the synthesized and adjusted mechanisms	53
4.2	Transmission angle η vs. ψ	54
4.3	Transmission angle ν vs. ψ	55
4.4	Rendering of the kinematic chain of the optimum spherical Stephenson mechanism	55
4.5	Spherical Stephenson mechanism with a streamlined coupler link	56
4.6	Mirror image of the optimum spherical Stephenson mechanism	56
4.7	The four Stephenson mechanisms upon assembly	57
4.8	Final embodiment of the solution mechanism	57
4.9	Embodiment of the spherical Stephenson mechanism	58
4.10	The shaping of the coupler link	58
4.11	Preliminary concept of the structure that will support the four	
	Stephenson mechanisms	59
4.12	Lamé curves for $p = 4$, $p = 6$ and $p = 8$	61
4.13	Curvature κ vs. x for Lamé curves with exponents $p=4, p=6$	
	and $p = 8 \ldots \ldots \ldots \ldots \ldots$	62
4.14	Side view of the designed cover based on Lamé curves	62
4.15	The assembly of the cover	63
4.16	Final embodiment with the design of the cover	63
4.17	Embodiment of the complete pitch-roll wrist	64

LIST OF TABLES

3.1	Numerical results of the weighted nonlinear least-square optimization	51
4.1	Synthesized and adjusted dimensions of the spherical Stephenson	
	mechanism	2

CHAPTER 1

Introduction

1.1. Background

The aim of this work is to optimize the epicyclic transmission of spherical camroller pairs, to be used as a pitch-roll wrist for a robotic manipulator or as a toolholder for a machine tool. In current industrial robots the design used to produce pitch-and-roll motions of a gripper is a differential mechanism that has two inputs and two outputs, the outputs being the pitch and the roll motions of the gripper. This differential mechanism is based on bevel gears and consists of two sun gears and one planet, carrying the gripper as shown in Fig. 1.1.

An epicyclic transmission of spherical cam-roller pairs, is being developed at McGill University's Centre for Intelligent Machines (Ghuneim, Angeles and Bai, 2004), and is based on the innovative design concept of Speed-o-Cam (González-Palacios and Angeles, 1999). This is a new generation of mechanical transmissions that offers advantages such as low friction, low backlash, high stiffness and manufacturability with general-purpose CNC machine tools.

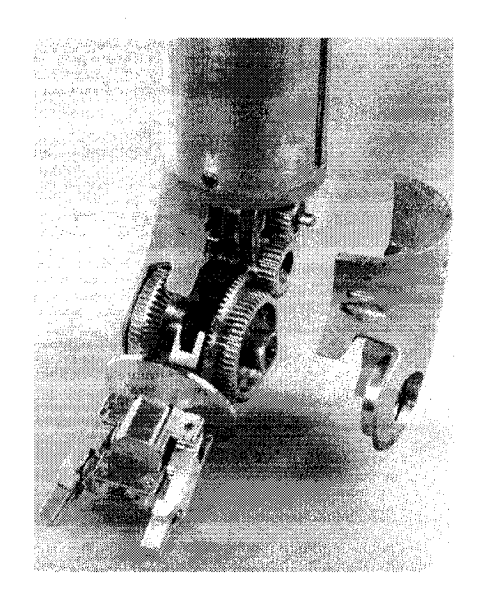


FIGURE 1.1. Wrist from a Remote-Control Manipulator (Rosheim, 1989)

The research leading to Speed-o-Cam has been undertaken at the Centre for Intelligent Machines (González-Palacios and Angeles, 1999) for the past few years. Prototypes of planar and spherical Speed-o-Cam transmissions are shown in Figure 1.2.

Figure 1.3 shows the first epicyclic transmission of spherical cam-roller pairs developed at McGill University, as designed by Ghuneim (2003). This mechanism has two input shafts driven by one motor each, its two outputs being the pitch and the roll motions of the wrist. The wrist of Fig. 1.3 can realize an arbitrary pitch-roll gesture with unlimited mobility on both the pitch and the roll axes. The gestures can

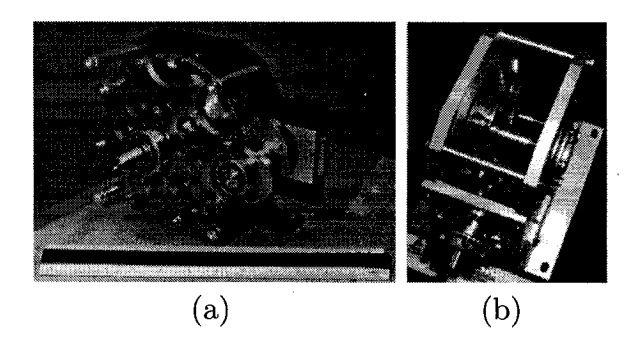


FIGURE 1.2. Planar (a) and Spherical (b) Speed-o-Cam prototypes

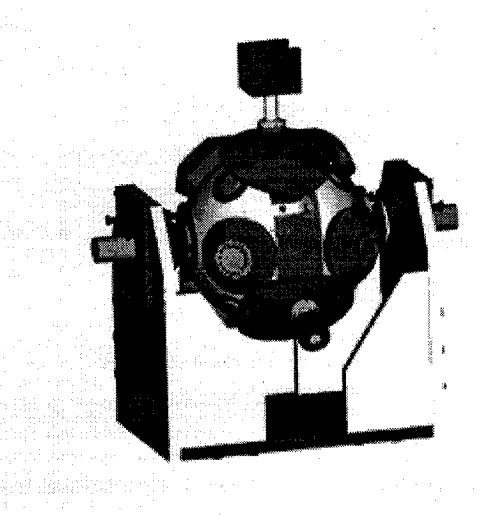


FIGURE 1.3. Epicyclic mechanism based on cam-roller pairs

be achieved, moreover, by controlling the velocity of the two motors. This mechanism has the features below:

- Cam-roller coupling;
- all links undergo spherical motion;
- the roller-carrying disks play the role of sun gears, the conjugate-cam subassemblies playing the roll of the rolling-and-pitching planets. In this mechanism the cam is the driven element;
- three conjugate cam subassemblies are used, located 120° apart, such that the mechanism is dynamically balanced;
- each camshaft undergoes three turns for every turn of the roller-carrying disk;
- each conjugate-cam subassembly consists of one shaft and two conjugate cams; the latter are mounted on a common shaft 180° out of phase, so as to ensure cam-roller contact all the time.

This new concept is intended to replace gripper drives based on bevel-gears transmissions.

1.2. Literature Review

Robotic wrists are commonly used in manipulators that require a large dextrous workspace (Cohen, Lipton, Dai and Benhabib, 1992; Howard, 2002; Rauchfuss and Yang, 2000; Yang, Lin and Cheng, 1990; Yang and Rauchfuss, 2001). The earliest pitch-roll wrists were developed by Raymond C. Goertz in the late 1940s and 1950s at Argonne National Laboratory with the purpose of handling nuclear materials (Rosheim, 1989). This device used sets of bevel gears for driving pitch and roll end-effector motion. This classic design is still used to design robotic wrists. In industry, robotic wrists like the Cincinnati Milacron T³ and the Bendix wrist were designed with bevel-gear trains in a differential array (Tsai, 1988). Planetary bevelgear trains can be adopted to produce spherical wrist mechanisms. Straight-tooth bevel-gear spherical wrist mechanisms have advantages like simple kinematics and low manufacturing cost, but due to their inherent sliding, they produce noise and vibration. Spiral-tooth gears can be used in order to avoid these drawbacks (Gosselin and Cloutier, 1993), at the expense of an unaffordably high cost. New concepts of robotic wrists that are not based on gear trains have been developed, like the robotic wrist reported by Wiitala and Stanisic (2000), which was designed based on a symmetrically actuated spherical eight-bar linkage; this linkage can eliminate the singularity within its hemispherical workspace. Another concept is the Agile Wrist, a three degree-of-freedom parallel spherical robotic wrist made up of a moving platform and a fixed based connected by three identical legs using revolute joints (Bidault, Angeles and Teng, 2001). This design took the concept of the three-degree-of-freedom Agile Eye designed by Gosselin and Hamel (1994). At McGill University, a robotic pitch-roll wrist is being developed based on spherical cam-roller pairs (Ghuneim, 2003; Ghuneim, Angeles and Bai, 2004). An improvement of that concept is reported in this thesis, in which we aim at replacing the three conjugate-cam subassemblies by an alternative mechanism that consists of a layout of two pairs of spherical Stephenson mechanisms and only two conjugate cams with a convex profile mounted on different shafts.

Most of the research work on spherical-linkage synthesis has focused on the spherical four-bar linkage (Ge and Larochelle, 1999; Ge and McCarthy, 1991; Zanganeh and Angeles, 1994), but work on spherical Stephenson mechanisms and spherical five-bar linkages is rather scarce. In this thesis the design of spherical Stephenson mechanisms is based on the method proposed by Wampler (2004), who formulates and solves the loop equations for indecomposable spherical structures with up to three loops.

In spherical cam-follower mechanisms, the axes of motion of the cam and the follower are concurrent (Angeles and López-Cajún, 1991). To preserve concurrency, the manufacturing errors in the production of the spherical cams should be low, to guarantee a good performance of the mechanism. As reported by Lee (2001), when machining a concave cam profile, the accuracy of the concave part was substantially lower than that of the convex regions; hence, a fully-convex cam profile should be targeted. The research work on spherical cams has mainly focused on the determination of the cam profile, as reported by Yang (2001), who derived a general expression based on envelope theory for the surface geometry of spherical cams with a meshing follower. Work on the manufacturing of spherical cams was reported recently by Wei, Lai and Chen (2000), who derived the equations of the cam profile based on the theory of conjugate surfaces to generate the associated NC data for a five-axis CNC machine tool, to produce a spherical cam-oscillating roller-follower mechanism. A literature survey showed a lack of results on the synthesis of spherical convex cam profiles and

their impact on the manufacturing accuracy of the cam. We thus undertook the derivation of a condition that guarantees a fully-convex cam profile.

1.3. Motivation

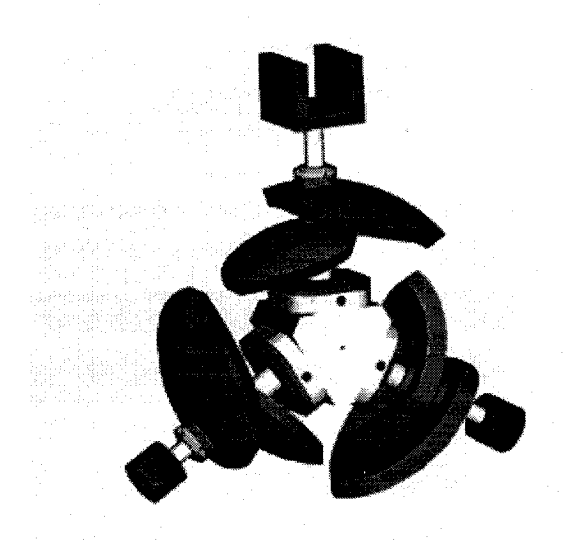


FIGURE 1.4. Hub with three conjugate cam subassemblies

Figure 1.4 shows the hub of Ghuneim's mechanism, carrying three conjugate-cam subassemblies. For assembly, it is necessary to machine the two conjugate cams and their shaft from one single blank, but this machining is close to impossible with the above array. Machining the cams from separate blanks is not an attractive option because of the inherent assembly error incurred. Therefore, an alternative mechanism comprising four spherical mechanisms of the Stephenson type is proposed here, in order to avoid the use of two conjugate cams mounted on a common shaft. The layout of the alternative mechanism is shown in Figure 1.5.

The alternative mechanism consists of two pairs of spherical Stephenson mechanisms, one pair forming the main mechanism (M), the other being its mirror image (I). The two pairs are arranged in such a way that the two output links of the two main

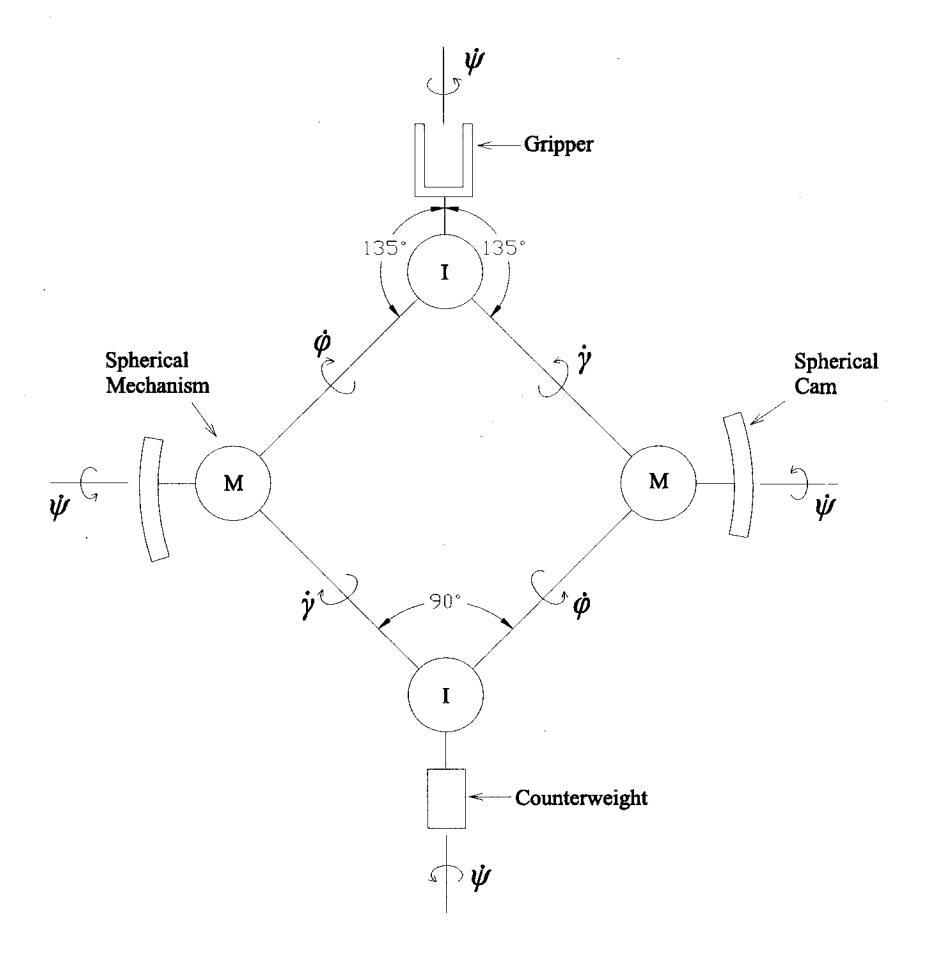


FIGURE 1.5. Layout of the alternative mechanism

mechanisms are connected to their corresponding output links in the mirror image mechanisms, in order to transmit the same motion at the same angular velocity. It is necessary to connect between the two main mechanisms a mirror-image mechanism, with the purpose of having the same angular velocity at the input shaft of the two main mechanisms. In order to have a symmetric layout, moreover, the input shaft of each of the two pairs of mechanisms makes an angle of 135° with each of their output shafts. Closing the loop, the whole arrangement has one degree of freedom.

The input shafts of the two main mechanisms rotate with the same angular velocity, but in directions opposite those of the input shafts of the two mirror-image mechanisms.

The input shafts of the two main mechanisms are connected to the cams. These two cams are conjugate, 180° out of phase, as mounted on different shafts. Regarding the two input shafts of the two mirror-image mechanisms, one is connected to the gripper and the other to a counterweight for purposes of static balancing.

This transmission mechanism requires only two conjugate cams, on different shafts; in the design of Fig. 1.3, on the contrary, three shafts with two conjugate cams are mounted on each shaft, the device thus requiring six cams.

This configuration requires two identical pairs of spherical Stephenson mechanisms, each pair composed of one such mechanism and its mirror image.

The above work requires extremely tight tolerances because of the presence of conjugate cams, the need for an even distribution of manufacturing errors in the production of spherical cams thus becoming apparent. Indeed, measurements on planar cams have revealed that the highest errors are encountered in regions with large curvature variations, especially in regions with a concavity (Lee, 2001). Due to the pronounced change in curvature that a concavity in the cam profile entails, the accuracy of the concave part is substantially lower than that of convex regions. We thus adopt as a criterion to evenly distribute the machining errors the avoidance of contact surfaces with negative geodetic curvature (Chiang, 1988). With the aim of avoiding spherical cams with sign changes in the geodetic curvature of the contact surface, which thus gives rise to a concave region, we propose a procedure based on curvature analysis that allows us to obtain fully-convex spherical cams. To be true, convexity refers here to the conical contact surface of the cam. Since we are interested in obtaining a fully-convex spherical cam, we impose a condition guaranteeing that the geodetic curvature of the cam remains positive.

The Synthesis of the Spherical Cam Mechanism

The machining of spherical cams is done with five axis CNC machine tools. Because of their speed of response, characterized by their bandwidth, these machines do not react fast enough under high changes of curvature in the workpiece.

Because the motion of cam mechanisms is determined by the contact between cam and follower, the profile accuracy turns out to be extremely important. For example, for good valve train dynamics, the cutting accuracy is of the order of 0.00020" (5.08 μ m), point to point for 1° cam rotation, with an overall tolerance of ± 0.0020 " (50.8 μ m) (Jensen, 1987).

Large fluctuations of the manufacturing errors were reported (Lee, 2001) in the production of the first prototype of a planar Speed-o-Cam (SoC), in which the cam had a concavity in its profile. The convex region of the cam exhibited a maximum error of 0.5 μ m, while the concave region exhibited a maximum error of 2.5 μ m. This indicates a machining error in the concave region of 500% that in the convex region. Our aim here is thus to avoid concavities in the contact surface of the cam.

To avoid machining a spherical cam profile with a concavity, we develop the condition that guarantees a *fully-convex spherical cam profile*.

2.1. Spherical Cam Mechanisms

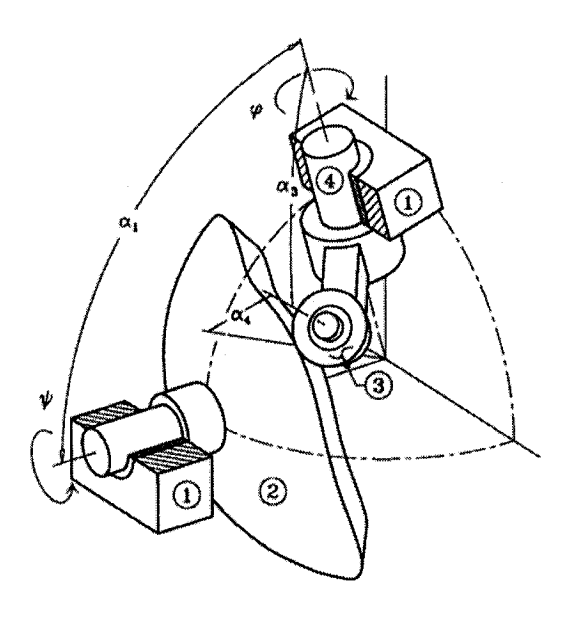


FIGURE 2.1. General layout of a spherical cam mechanism with a roller-follower [taken from (González-Palacios and Angeles, 1993)]

Figure 2.1 shows the general layout of a *spherical cam mechanism* with a roller-follower of the conical type, which guarantees a pure rolling operation. The contact surface of the cam is a conic surface generated by a ray stemming from the centre of the sphere, as it traverses the generatrix of the cam profile (González-Palacios and Angeles, 1993).

This type of mechanism is composed of four links: (1) the frame; (2) the cam; (3) the roller; and (4) the follower. The geometric parameters defining the spherical cam mechanism are:

- (i) The angle α_1 between the input and output axes.
- (ii) The angle α_3 between the output and roller axes.

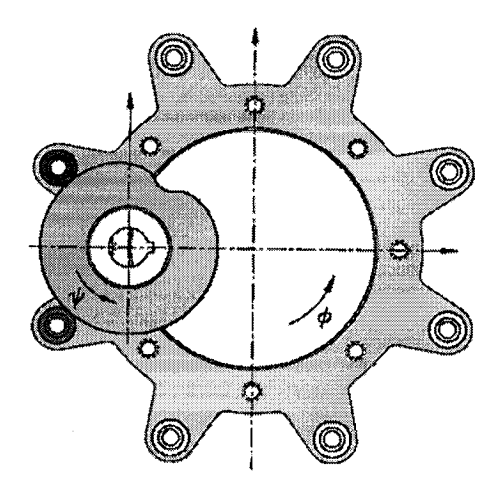


FIGURE 2.2. An Indexing Cam Mechanism

(iii) The angle α_4 between the roller cone.

Speed-o-Cam mechanisms have the morphology of Indexing Cam Mechanisms (ICM). As shown in Figure 2.2, an ICM consists of one cam and multiple rollers carried by a follower. When a roller comes into contact with the cam, it forms a temporary single cam mechanism; when the roller loses contact with the cam, another roller begins to engage the cam, thereby keeping the follower under motion all the time.

In order to transmit motion continuously to the output shaft of the transmission, moreover, the whole mechanism is made of two conjugate cams 180° out of phase, as shown in Fig. 2.3.

The input-output relation of the spherical Speed-o-Cam takes the form

$$\phi = \frac{\pi}{N} \left(N - 1 + \frac{\psi}{\pi} \right)$$

where

N: number of rollers (number of indexing steps).

 ψ : angle of rotation of the cam.

 ϕ : angle of rotation of the follower.

2.2. Curvature Analysis

The contact surface of the cam is a conic surface produced by a ray stemming from the center of the sphere, as it traverses the *generatrix* Γ of the cam profile. Moreover, the roller becomes a frustroconic surface of cone angle α_4 (González-Palacios and Angeles, 1993). The *geodetic curvature* κ of a curve Γ on a spherical surface is given by (Chiang, 1998)

$$\kappa = \frac{\mathbf{e}^T(\mathbf{e}' \times \mathbf{e}'')}{\parallel \mathbf{e}' \parallel^3} \tag{2.1}$$

where e is the unit position vector of a point on the generatrix lying on the surface of the *unit sphere*, while (') and (") indicate first and second derivatives with respect to a parameter. The geodetic curvature is also defined as (Chiang, 1998),

$$\kappa = \frac{1}{\tan \rho} \tag{2.2}$$

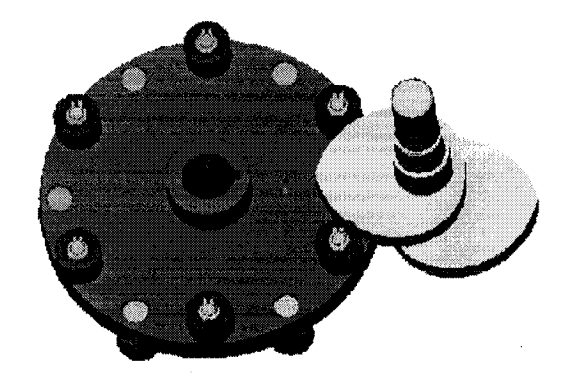


FIGURE 2.3. Indexing mechanism with two conjugate cams 180° out of phase

where ρ is the spherical radius of curvature that takes the value of the angle subtended by the arc of the great circle starting from the center of curvature to the curve. By definition, from eq.(2.2), the geodetic curvature κ turns out to be dimensionless.

In our case, the natural choice to parametrize the cam generatrix is the angle ψ of rotation of the cam, which is shown in Fig. 2.1. From eq.(2.1) it is apparent that the derivatives of the cam profile with respect to the input angle ψ will be needed. Based on the spherical mechanism shown in Fig. 2.1, the unit vector \mathbf{e}_c of the cam profile and the unit vector of the pitch curve \mathbf{e}_p are defined as

$$\mathbf{e}_c = \mathbf{S}(\psi)\mathbf{Q}(\alpha_1)\mathbf{S}^T(\phi)\mathbf{Q}(\alpha_3)\mathbf{S}(\nu)\mathbf{Q}(\alpha_4)\mathbf{k}$$
 (2.3)

$$\mathbf{e}_{p} = \mathbf{S}(\psi)\mathbf{Q}(\alpha_{1})\mathbf{S}^{T}(\phi)\mathbf{Q}(\alpha_{3})\mathbf{k}$$
 (2.4)

where **Q** and **S** represent rotation matrices about the X and Z axes, respectively, through angles given by their arguments, and $\mathbf{k} = [0 \ 0 \ 1]^T$. To carry out an analysis of curvature we can see in eqs.(2.3) and (2.4) that the expression for the unit vector \mathbf{e}_c of the cam profile is not as simple to handle as that of the pitch curve \mathbf{e}_p .

Now, the spherical radius of curvature of the pitch curve ρ_p is equal to the sum of the spherical radius of curvature of the cam profile ρ_c and the spherical radius of the roller r, as indicated in Fig. 2.4, i.e.,

$$\rho_p = \rho_c + r \tag{2.5}$$

From eq.(2.5) the relation between the curvatures of the pitch curve κ_p and the cam profile κ_c are expressed as

$$\kappa_p = \frac{\kappa_c - \tan r}{1 + \kappa_c \tan r} \tag{2.6}$$

As a consequence of the relations appearing in eqs.(2.5) and (2.6), a convex pitch curve guarantees a convex cam profile. Hence, we will work with the generatrix of the pitch curve, rather than with the cam profile, in the ensuing analysis.

From eq.(2.4), e_p reduces to

$$\mathbf{e}_{p} = \begin{bmatrix} (\sin \alpha_{1} \cos \alpha_{3} + \cos \alpha_{1} \sin \alpha_{3} \cos \phi) \sin \psi - \sin \alpha_{3} \cos \psi \sin \phi \\ -(\sin \alpha_{1} \cos \alpha_{3} + \cos \alpha_{1} \sin \alpha_{3} \cos \phi) \cos \psi - \sin \alpha_{3} \sin \psi \sin \phi \\ \cos \alpha_{1} \cos \alpha_{3} - \sin \alpha_{1} \sin \alpha_{3} \cos \phi \end{bmatrix}$$
(2.7)

2.3. Cam-Profile Determination

In order to create a curve in CAD software, then integrating it into the CNC machine-tool code, we need to obtain the range of ψ values that produce a fully-closed cam profile. This interval is determined by the angle Δ (Lee, 2001), as shown in Fig. 2.5, depicting a symmetric profile. Symmetry is natural here because of the function of the mechanism, which is identical to that of bevel gears. The angle ψ takes

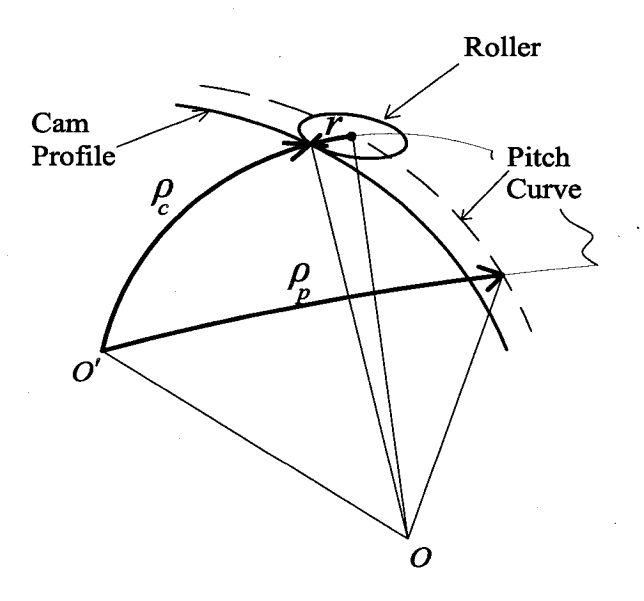


FIGURE 2.4. Spherical radius of curvature

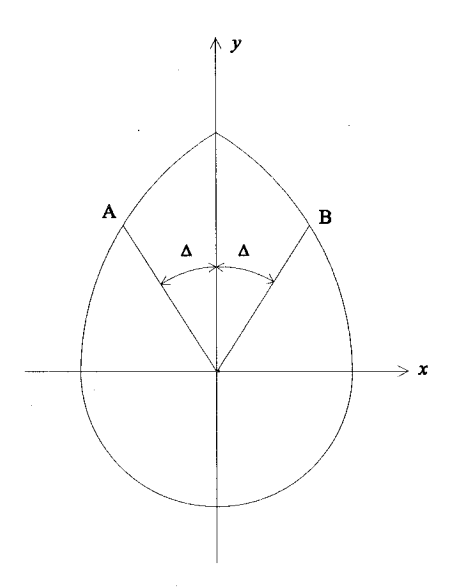


FIGURE 2.5. A sketch of the cam profile geometry

on values in the interval $[0, 2\pi]$, with the value $\psi = 0$ at the point A of engagement and the value $\psi = 2\pi$ at the point B of disengagement, as illustrated in Fig. 2.5.

From eq.(2.7) the variables x and y take the values of the first and second components, respectively, that are the X and Y components of the position vector \mathbf{e}_p of the pitch curve, namely,

$$x(\psi) = (\sin \alpha_1 \cos \alpha_3 + \cos \alpha_1 \sin \alpha_3 \cos \phi) \sin \psi - \sin \alpha_3 \cos \psi \sin \phi$$

$$y(\psi) = -(\sin \alpha_1 \cos \alpha_3 + \cos \alpha_1 \sin \alpha_3 \cos \phi) \cos \psi - \sin \alpha_3 \sin \psi \sin \phi$$

Realizing that y is the axis of symmetry of the cam profile from Figure 2.5, we can obtain Δ by setting:

$$x(\Delta + 2\pi) = 0 \tag{2.8}$$

Taking $x(\Delta + 2\pi)$ equal to the first row of eq.(2.7) and simplifying trigonometrically, we obtain

$$x(\Delta + 2\pi) = (\sin \alpha_1 \cos \alpha_3 + \cos \alpha_1 \sin \alpha_3 \cos \phi(\Delta + 2\pi)) \sin \Delta - \sin \alpha_3 \sin \phi(\Delta + 2\pi) \cos \Delta = 0$$

Let

$$f(\Delta) = (\sin \alpha_1 \cos \alpha_3 + \cos \alpha_1 \sin \alpha_3 \cos \phi(\Delta + 2\pi)) \sin \Delta - \sin \alpha_3 \sin \phi(\Delta + 2\pi) \cos \Delta$$

To find the roots Δ of $f(\Delta)$, we resort to the Newton-Raphson method, namely, for initial guess Δ_0 ,

$$\Delta_i = \Delta_{i-1} - \frac{f(\Delta_{i-1})}{f'(\Delta_{i-1})} \tag{2.9}$$

where

$$f'(\Delta) = (\cos \alpha_1 \sin \alpha_3 \sin \Delta \sin \phi(\Delta + 2\pi) + \sin \alpha_3 \cos \Delta \cos \phi(\Delta + 2\pi)) \phi'(\Delta + 2\pi)$$

$$+ (\sin \alpha_1 \cos \alpha_3 + \cos \alpha_1 \sin \alpha_3 \cos \phi(\Delta + 2\pi)) \cos \Delta \qquad (2.10)$$

$$+ \sin \alpha_3 \sin \phi(\Delta + 2\pi) \sin \Delta$$

This procedure stops when $\|\Delta_i - \Delta_{i-1}\| \le \epsilon$, for a prescribed tolerance ϵ . Once the value of Δ is found, the cam profile is closed, with $\psi_{min} = -\Delta$ and $\psi_{max} = 2\pi + \Delta$, i.e.,

$$-\Delta = \psi_{min} < \psi < \psi_{max} = 2\pi + \Delta$$

and hence, ψ takes on values in the interval $[-\Delta, 2\pi + \Delta]$.

2.4. Convexity Condition

The conic contact surface of a cam profile shows a concavity if the geodetic curvature of the pitch curve Γ changes its sign, which happens when the numerator of the geodetic curvature vanishes. The condition for a convex cam profile is, therefore, that the numerator of the geodetic curvature do not change its positive sign, i.e.,

$$\mathbf{e}^T(\mathbf{e}' \times \mathbf{e}'') \ge 0 \tag{2.11}$$

To obtain an expression for the convexity condition we substitute the unit vector of the pitch curve \mathbf{e}_p into eq.(2.11), the first and second derivatives of this vector

being found with computer algebra, which yields the expression

$$F(\psi) \equiv A\cos^3\phi + B\cos^2\phi + C\cos\phi + D \ge 0 \tag{2.12}$$

where

$$A = \sin^3 \alpha_1 \sin^3 \alpha_3$$

$$B = 3\sin^2 \alpha_1 \cos \alpha_3 \ (\phi' \sin^2 \alpha_3 + \cos \alpha_1 \cos^2 \alpha_3 + \cos \alpha_1)$$

$$C = \sin \alpha_1 \sin \alpha_3 \ \phi'^2 (1 - 3\sin^2 \alpha_3)$$

$$+ 3\cos \alpha_1 \sin \alpha_1 \sin \alpha_3 \ \phi' \ (2\sin^2 \alpha_3 - 1)$$

$$+ \sin \alpha_1 \sin \alpha_3 \ (3\cos^2 \alpha_1 \cos^2 \alpha_3 - 1)$$

$$D = \sin \phi \sin \alpha_1 \sin \alpha_3 \ \phi'' - \sin^2 \alpha_3 \cos \alpha_3 \ \phi'^3$$

$$+ 3\cos \alpha_1 \sin^2 \alpha_3 \cos \alpha_3 \ \phi'^2$$

$$+ \cos \alpha_1 \cos \alpha_3 \ (1 - \cos^2 \alpha_1 \cos^2 \alpha_3)$$

We call eq.(2.12) the convexity condition for spherical cams. This expression is apparently given in terms of the cosine of the input-output function $\phi(\psi)$.

A cam contact surface is thus *convex* if and only if $F(\psi)$ of eq.(2.12) is non-negative for any real value of ψ .

2.4.1. Concavity-Occurrence in the Cam Profile If the geodetic curvature of the cam vanishes and a change in sign is produced, then a concavity in the cam profile arises. To find the value of ψ at which the concavity occurs, we need the roots of $F(\psi)$, with $F(\psi) = 0$ defined in the convexity condition eq.(2.12), thereby deriving a cubic polynomial equation in $\cos \phi$, namely,

$$F(\psi) \equiv A\cos^3\phi + B\cos^2\phi + C\cos\phi + D = 0$$

To find the roots of the above equation, let $\cos \phi \equiv x$ which yields

$$A x^3 + B x^2 + C x + D = 0 (2.13)$$

From eq.(2.12) it is apparent that the coefficient A never vanishes because the values of α_1 and α_3 are bounded as: $0 < \alpha_1 \le 90^\circ$ and $0 < \alpha_3 \le 90^\circ$; therefore, we can safely normalize eq.(2.13) upon dividing its two sides by A, thus obtaining

$$f(x) = x^3 + \frac{B}{A} x^2 + \frac{C}{A} x + \frac{D}{A} = 0$$
 (2.14)

There can be up to three real roots for this polynomial, each root defining two values of ψ . The real roots of the polynomial lie in the interval [-1,1]. To find the number of real roots of a polynomial in a given interval we recall *Sturm's theorem* (Merlet, 1993): Let $f_0(x) = 0$ be a polynomial of degree n in x

$$f_0(x) = \sum_{i=0}^{n} a_i x^i = 0$$

Considering the first derivative of this polynomial with respect to x,

$$f_1(x) = f_0'(x)$$

the number of real roots of the equation f(x) = 0 in the interval $[x_1, x_2]$ is obtained as the number of sign changes in the sequence $f_i(x_1), f_{i+1}(x_1), i \in [0, n-1]$ minus the number of sign changes in the sequence $f_i(x_2), f_{i+1}(x_2), i \in [0, n-1]$.

Figure 2.6a shows the synthesized cam profile of a Speed-o-Cam mechanism with $\alpha_1 = 90^{\circ}$, $\alpha_3 = 80^{\circ}$ and N = 8. For those values, the cam profile exhibits a concavity in the interval 151.74° $\leq \psi \leq 208.26^{\circ}$. From Fig. 2.6b we can see that the geodetic curvature vanishes and changes its sign.

Figure 2.7a shows the synthesized cam profile of a Speed-o-Cam mechanism with $\alpha_1 = 90^{\circ}$, $\alpha_3 = 73^{\circ}$ and N = 8. For those values the cam profile is fully convex. In

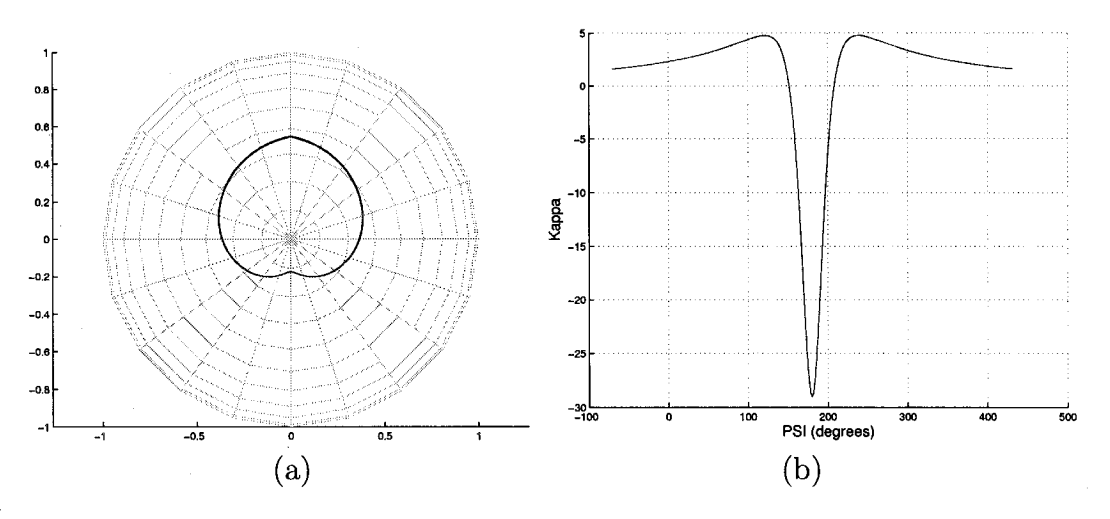


FIGURE 2.6. Synthesized concave cam (a) and its geodetic curvature (b)

Fig. 2.6b we can see that the geodetic curvature of the convex cam profile does not vanish.

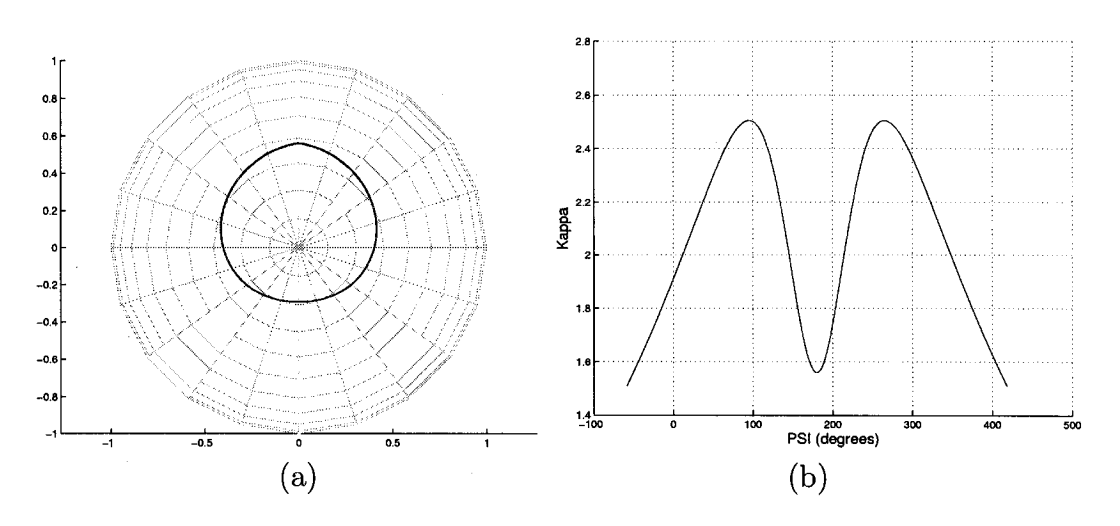


FIGURE 2.7. Synthesized convex cam (a) and its geodetic curvature (b)

From Figures 2.6b and 2.7b we can observe that the concave cam profile has a higher change of curvature with a peak-to-peak value of 33.79, vs. 0.95 for the convex cam profile.

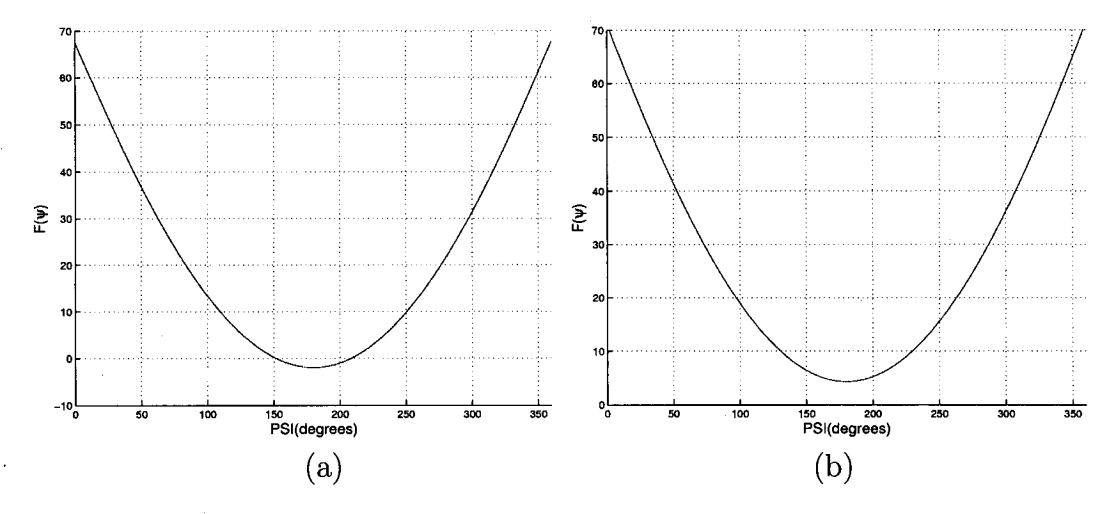


FIGURE 2.8. Convexity condition $F(\psi)$ vs. ψ : (a) for the concave cam; and (b) for the convex cam

Figure 2.8 shows the plots of the convexity condition $F(\psi)$ vs. ψ of the synthesized concave and convex cams. From Fig. 2.8a notice that $F(\psi)$ reaches negative values, which indicates the concavity in the profile.

Figure 2.9 shows the cam profile generated in PRO/ENGINEER for the convex profile.

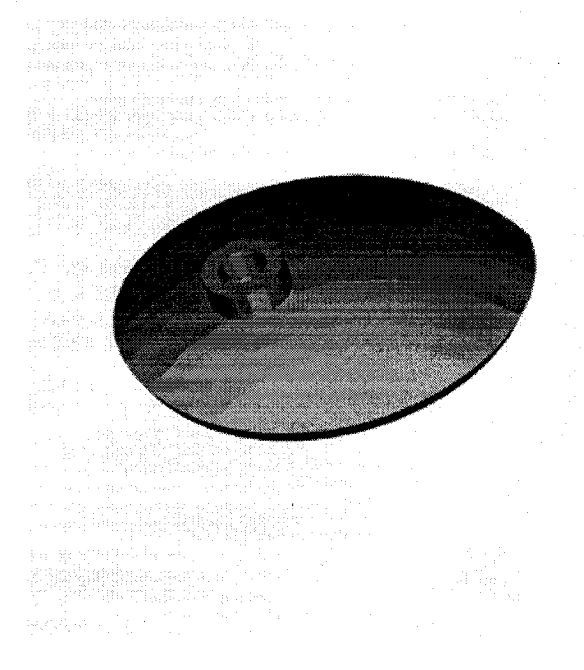


FIGURE 2.9. Convex cam profile

The Optimum Synthesis of a Spherical Stephenson Mechanism

In order to avoid the use of two conjugate cams mounted on the same shaft of the epicyclic transmission of Fig. 1.3, we develop here an alternative mechanism. This mechanism is intended to replace the hub that carries the conjugate-cam subassemblies of that epicyclic transmission. The layout of the alternative mechanism is shown in Fig. 1.5. This mechanism consists of two pairs of spherical Stephenson mechanisms, one pair being the main mechanism (M), the other its mirror image (I). From Fig. 1.5 we can see that the two output links of the two main mechanisms are connected to the corresponding output links of the mirror-image mechanisms in order to transmit the same motion at the same angular velocity. This arrangement has the peculiarity that the input shafts of the two main mechanisms rotate with the same angular velocity but in a direction opposite that of the input shafts of the two mirror-image mechanisms.

To create a symmetric layout, the input shaft of each of the two pairs of mechanisms makes an angle of 135° with respect to each of their output shafts.

Using this layout, the design of the mechanism will simplify: Instead of designing four spherical Stephenson mechanisms, we design only one mechanism; its mirror image is used for the second pair.

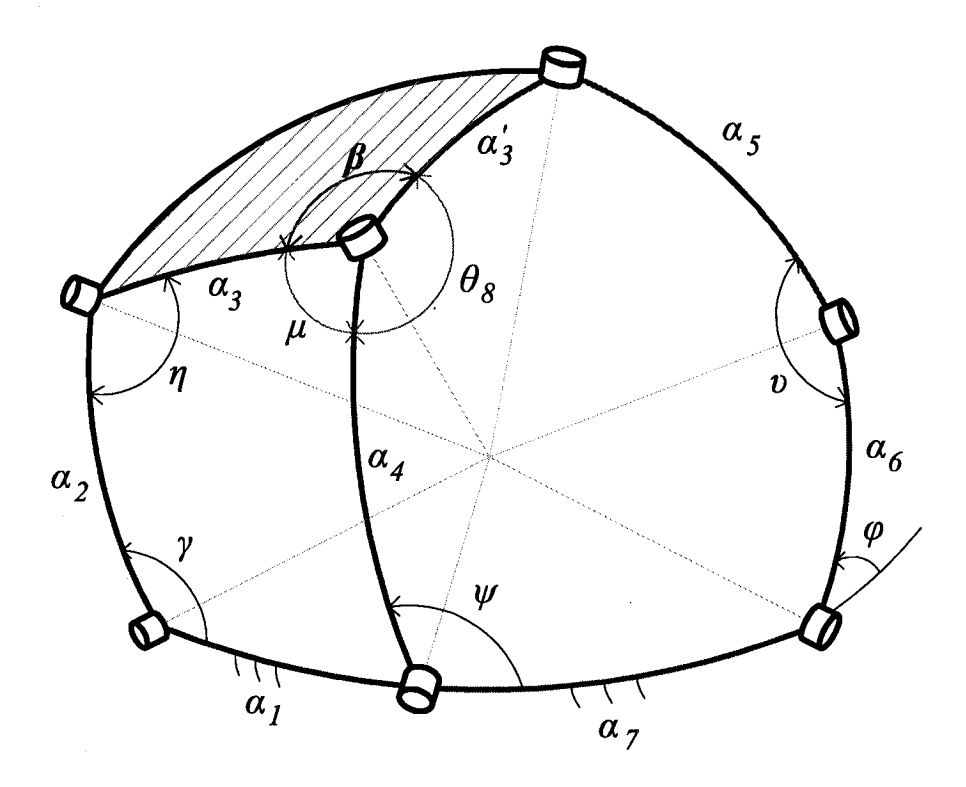


FIGURE 3.1. Spherical Stephenson mechanism

In order to design the spherical Stephenson mechanism of interest, we resort to the synthesis equations of its four- and five-bar loops; then, we proceed finding a single input-output (IO) equation that contains the input and the two output angles as well as the mechanism link dimensions. This procedure is reported in the sections below.

3.1. The Spherical Stephenson Mechanism

The classical Stephenson mechanism is a six-bar planar linkage that was originally designed to control the motion of a steam engine (Primrose, Freudenstein and Roth, 1967). The kinematic chain of a spherical Stephenson mechanism is illustrated in Fig. 3.1. This mechanism comprises six links connected by seven revolute joints; laid out in two loops, the four-bar loop (left-hand side) and the five-bar loop (right-hand side) are coupled by means of a ternary link. This mechanism is known to have a

single degree of freedom, hence, one single input joint drives the mechanism. For the sake of conciseness, we refer to the various binary links by the labels of the arcs that define every such link. Due to our design requirements, we chose the link α_4 as the input link and the links α_2 and α_6 as the output links.

For the layout shown in Fig. 1.5, the four spherical Stephenson mechanisms make up a total of 24 links, but we need to consider that four of the links are counted twice, and that the fixed link is common to all four mechanisms, the total number of links then being

$$l = 4(6) - 4 - 3 = 17$$

For the same layout, we have a total of 28 revolute joints, but four of these are counted twice, the total number of joints then being

$$j = 4(7) - 4 = 24$$

Using the Chebyshev-Grübler-Kutzbach (CGK) formula (Hervé, 1978; Angeles, 2003), to find the degree-of-freedom (dof) f of the layout, we have,

$$f = 6(17 - 1) - 5(24) = -24$$

However, the above result is wrong, for it predicts a hyperstatic structure, while the mechanism moves with a dof f = 1. To prove this, we recall, the *double Cardan* joint or *double universal joint* used in terrestrial vehicles, as illustrated in Fig. 3.2.

The double Cardan joint is used to transmit motion from the motor of the vehicle to the differential gear train, located in Fig. 3.2 inside the "load" block. As is well known, the entire mechanism depicted in Fig. 3.2 has a dof f = 1, which can be shown by resorting to group theory, as proposed by Hervé (1978).

In his 1978 paper, Hervé proposed a classification of mechanisms, for purposes of dof-determination, based on group theory. The concepts in this breakthrough paper

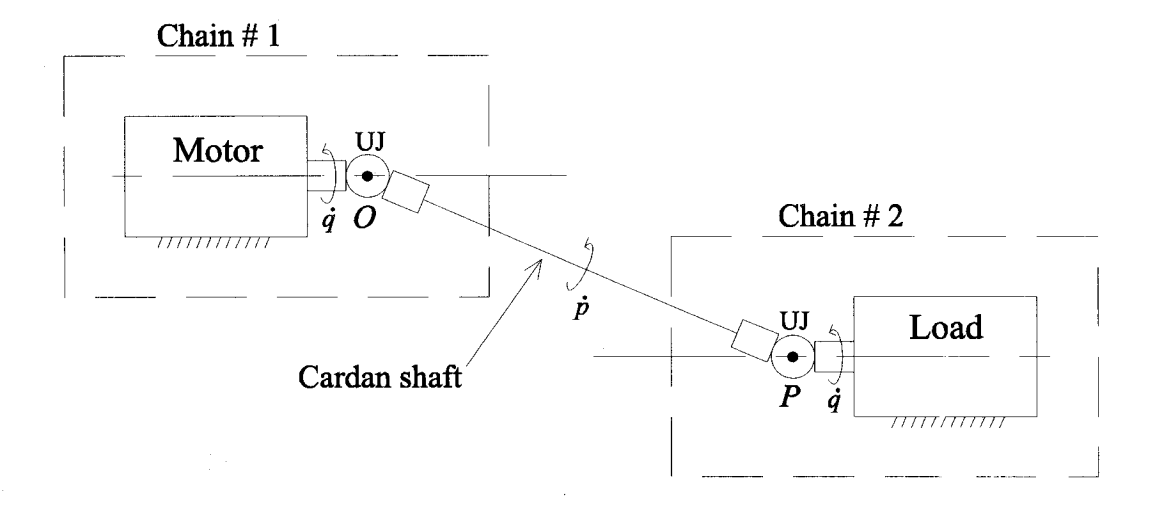


FIGURE 3.2. Double Cardan joint used in vehicles

have, unfortunately, remained unnoticed in the mechanisms community, probably because it was written in French. Hervé's classification is outlined in (Angeles, 1982). Accordingly, mechanisms are classified into

- (a) Trivial, when the mechanism links are all constrained to move with displacements belonging to one single displacement subgroup out of the 12 subgroups of the displacement group. These subgroups are the six generated by the corresponding lower kinematic pairs (Hartenberg and Denavit, 1964)—revolute, prismatic, screw, cylindrical, planar and spherical—plus other six resulting as combinations of the former: the planar translation; the spatial translation; the translating screw; the Schönflies subgroup; the identity subgroup; and the displacement subgroup itself.
- (b) Exceptional, when the mechanism links are all constrained to move with displacements (i) not belonging to one single proper subgroup¹, but rather to a set of subgroups, and (ii) the intersection of these subgroups is a subgroup. The dof of the mechanism, then, is the dimension of the intersection subgroup.

¹A proper subgroup of a group \mathcal{G} is any subgroup of \mathcal{G} , excluding \mathcal{G} itself.

(c) Paradoxical, when the mechanism links are all constrained to move with displacements including at least one subset that is not a subgroup. Examples of this class abound in the literature, namely, the Bennett linkage, the Bricard mechanism, the planar double-parallelogram linkage, etc. These mechanisms are sometimes referred to as maverick or overconstrained.

Under the above classification, it is now a simple matter to realize that the links of the double universal joint of Fig. 3.2 are constrained to move with displacements of two subgroups: the spherical subgroups with centres at O and P, respectively. The intersection of these two subgroups is that generated by the revolute of axis OP, whose dimension is unity, hence, under Hervé's classification, this is an exceptional mechanism. The double universal joint thus has a dof f = 1.

Following the same procedure as above, in order to find the dof of the layout of Fig. 1.5, we proceed first by separating the mechanism of the same figure into two chains, as shown in Fig. 3.3, chain # 2 being the mirror-image of chain # 1 with respect to a plane perpendicular to axes A_3 and A_4 , passing through the point of intersection of axes A_1 and A_2 . Chain # 1 contains a main spherical Stephenson mechanism M, interconnected to its mirror-image mechanism I via shaft S_1 . Since each spherical Stephenson mechanism has a dof f = 1 and the two are interconnected by the common shaft S_1 , chain # 1 has also a dof f = 1. The same occurs for chain # 2, which is the mirror-image of chain # 1, and is formed also by two spherical Stephenson mechanisms interconnected via shaft S_2 .

Now, each of the two subchains produced by the above cut having a single dof, it can be driven by one single input, namely, the angular velocity $\dot{\psi}$ of its camshaft, of axis A_2 . This subchain, then, has three outputs, those of A_1 , A_3 and A_4 . The two outputs about shaft A_4 are $\dot{\gamma}$, those about A_3 are $-\dot{\gamma}$. As a result, the two shaft pairs of axis A_3 and those of axis A_4 can be interconnected, for each pair is *compatible*. As a result, the interconnected mechanism of Fig. 1.5 is endowed with a single dof, and hence, can be driven with one single motor, driving either of the two shafts of

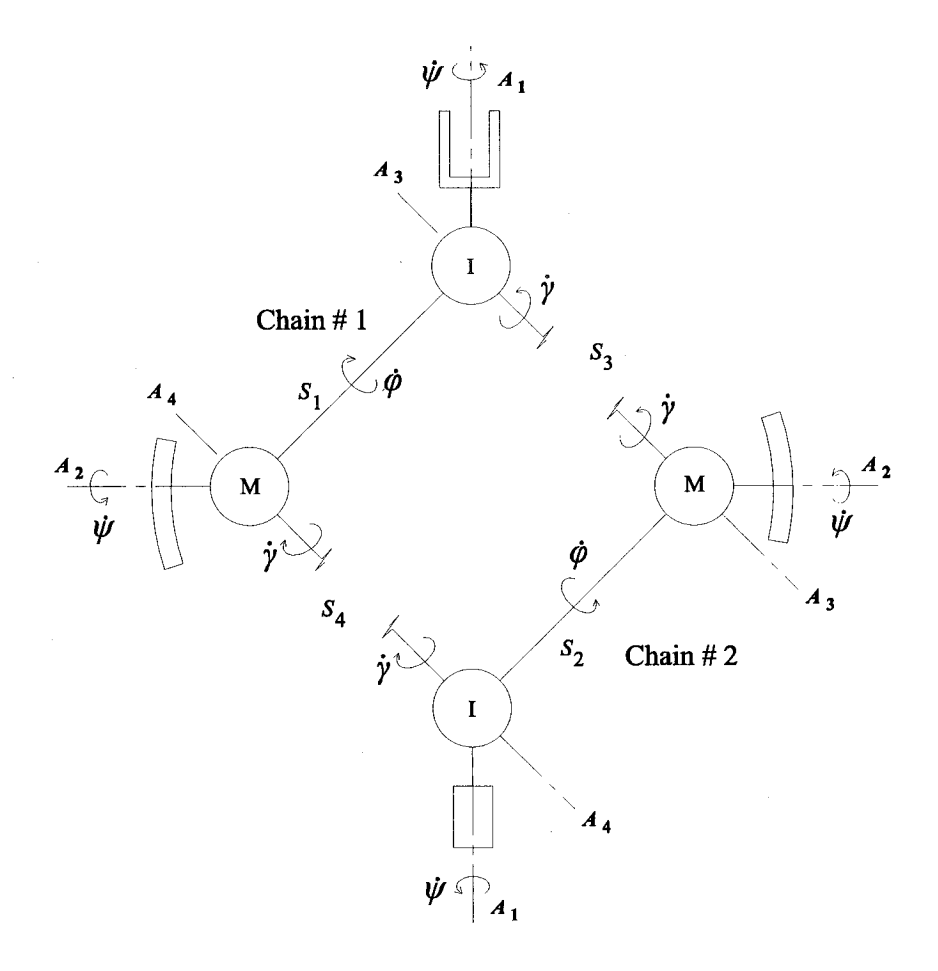


FIGURE 3.3. The layout of the alternative mechanism separated in two chains axis A_2 . As a matter of fact, in the pitch-roll wrist under design, these two shafts are driven by means of motions impinged to their cams by the rollers in contact with them and carried by the plates driven by the two wrist motors.

Below we explain the procedure used to obtain the equations of the four-bar and five-bar loops of this alternative mechanism.

3.2. Loop Equation

In order to find the four and five-bar loop equations, we resort to the method introduced by Wampler (2004). In this method, the first step is to define a set of coordinate axes at each joint aligning the z-axis with the axis of rotation of the joint.

The x and y axes can be given any orientation normal to z, so as to form a right-handed orthogonal coordinate system. The assumption that the links are rigid implies that the relative orientation between any two coordinate systems fixed to the same link is constant. Such rotations are called "side rotations" of the link. The x-axis is taken as the axis of rotation for the side rotations. In traversing a loop of a spherical mechanism, two types of rotations are found *joint rotations*, which are variable, and side rotations, which are constant. A typical loop matrix equation has the form

$$\mathbf{Z}_1 \mathbf{S}_1 \mathbf{Z}_2 \mathbf{S}_2 \dots \mathbf{Z}_{k-1} \mathbf{S}_{k-1} \mathbf{Z}_k \mathbf{S}_k = 1 \tag{3.1}$$

where \mathbf{Z}_i is a joint rotation about the z-axis, through angle θ_i , namely,

$$\mathbf{Z}_{i} = \begin{bmatrix} \cos \theta_{i} & -\sin \theta_{i} & 0 \\ \sin \theta_{i} & \cos \theta_{i} & 0 \\ 0 & 0 & 1 \end{bmatrix}$$

in link-fixed coordinates. Further, S_i is a side rotation about the x-axis, through angle α_i , namely,

$$\mathbf{S}_{i} = \begin{bmatrix} 1 & 0 & 0 \\ 0 & \cos \alpha_{i} & -\sin \alpha_{i} \\ 0 & \sin \alpha_{i} & \cos \alpha_{i} \end{bmatrix}$$

and 1 is the 3×3 identity matrix.

3.2.1. Rotation-Matrix Formulation The second step in Wampler's method is to eliminate the two joint rotations \mathbf{Z}_1 and \mathbf{Z}_k from the loop equation matrix, eq.(3.1), to end up with a single trigonometric loop equation.

Letting $\mathbf{z}_i = [0 \ 0 \ 1]^T$, we observe that $\mathbf{z}_i^T \mathbf{Z}_i = \mathbf{z}^T$ and $\mathbf{Z}_i \mathbf{z}_i = \mathbf{z}$, where $\mathbf{z} = [0 \ 0 \ 1]^T$. Thus, we can eliminate the two joint rotations, \mathbf{Z}_1 and \mathbf{Z}_k from eq.(3.1) upon multiplying its two sides by $\mathbf{S}_k^T \mathbf{z}_k$, and then multiplying the equation thus

resulting from the left by \mathbf{z}_1^T , namely,

$$\mathbf{z}_1^T \mathbf{Z}_1 \mathbf{S}_1 \mathbf{Z}_2 \mathbf{S}_2 \dots \mathbf{Z}_{k-1} \mathbf{S}_{k-1} \mathbf{Z}_k \mathbf{z}_k = \mathbf{z}_1^T \mathbf{S}_k^T \mathbf{z}_k$$

which can be readily simplified to yield

$$\mathbf{z}^T \mathbf{S}_1 \mathbf{Z}_2 \mathbf{S}_2 \dots \mathbf{Z}_{k-1} \mathbf{S}_{k-1} \mathbf{z} = \mathbf{z}_1^T \mathbf{S}_k^T \mathbf{z}_k$$
 (3.2)

the right-hand side being the (3,3) entry of S_k .

Equation (3.2) is the loop equation in trigonometric form.

3.3. The Four-Bar Loop

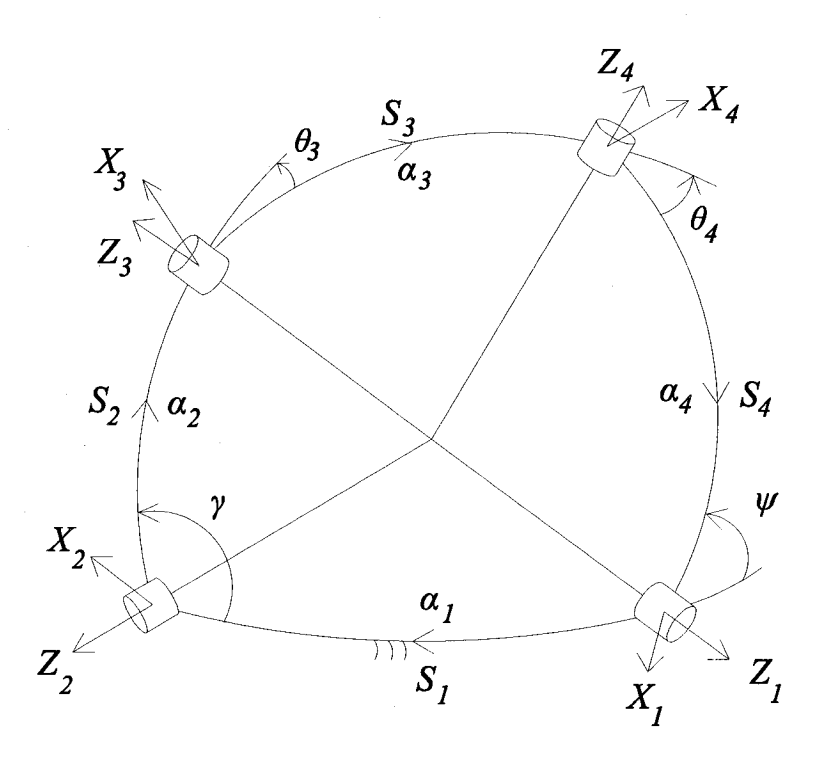


FIGURE 3.4. The four-bar loop

To find the four-bar loop equation based on Wampler's method we proceed by defining the coordinate axes at each joint, as shown in Fig. 3.4. To end up with a loop equation in trigonometric form as a function only of the input and output angles

 γ and ψ , respectively, we chose the loop equation so as to eliminate the two other joint angles. Hence, the loop equation is taken as

$$\mathbf{Z}_4 \mathbf{S}_4 \mathbf{Z}_1 \mathbf{S}_1 \mathbf{Z}_2 \mathbf{S}_2 \mathbf{Z}_3 \mathbf{S}_3 = \mathbf{1} \tag{3.3}$$

where

$$\mathbf{Z}_1 = \begin{bmatrix} \cos \psi & -\sin \psi & 0 \\ \sin \psi & \cos \psi & 0 \\ 0 & 0 & 1 \end{bmatrix}, \quad \mathbf{Z}_2 = \begin{bmatrix} -\cos \gamma & -\sin \gamma & 0 \\ \sin \gamma & -\cos \gamma & 0 \\ 0 & 0 & 1 \end{bmatrix}$$

$$\mathbf{Z}_{3} = \begin{bmatrix} \cos \theta_{3} & -\sin \theta_{3} & 0 \\ \sin \theta_{3} & \cos \theta_{3} & 0 \\ 0 & 0 & 1 \end{bmatrix}, \quad \mathbf{Z}_{4} = \begin{bmatrix} \cos \theta_{4} & -\sin \theta_{4} & 0 \\ \sin \theta_{4} & \cos \theta_{4} & 0 \\ 0 & 0 & 1 \end{bmatrix}$$

Wampler's method uses exterior angles at each vertex, instead of interior angles, matrix \mathbb{Z}_2 being a function of the interior angle γ . Moreover,

$$\mathbf{S}_{1} = \begin{bmatrix} 1 & 0 & 0 \\ 0 & \cos \alpha_{1} & -\sin \alpha_{1} \\ 0 & \sin \alpha_{1} & \cos \alpha_{1} \end{bmatrix}, \quad \mathbf{S}_{2} = \begin{bmatrix} 1 & 0 & 0 \\ 0 & \cos \alpha_{2} & -\sin \alpha_{2} \\ 0 & \sin \alpha_{2} & \cos \alpha_{2} \end{bmatrix}$$

$$\mathbf{S}_{3} = \begin{bmatrix} 1 & 0 & 0 \\ 0 & \cos \alpha_{3} & -\sin \alpha_{3} \\ 0 & \sin \alpha_{3} & \cos \alpha_{3} \end{bmatrix}, \quad \mathbf{S}_{4} = \begin{bmatrix} 1 & 0 & 0 \\ 0 & \cos \alpha_{4} & -\sin \alpha_{4} \\ 0 & \sin \alpha_{4} & \cos \alpha_{4} \end{bmatrix}$$

We eliminate the joint matrices \mathbb{Z}_3 and \mathbb{Z}_4 from eq.(3.3) to have the loop equation in terms of the input and output angles alone. We do this by means of the relation

$$\mathbf{z}_4^T \mathbf{Z}_4 \mathbf{S}_4 \mathbf{Z}_1 \mathbf{S}_1 \mathbf{Z}_2 \mathbf{S}_2 \mathbf{Z}_3 \mathbf{z}_3 = \mathbf{z}_4^T \mathbf{S}_3^T \mathbf{z}_3$$

whence the loop equation is obtained as

$$\mathbf{z}^T \mathbf{S}_4 \mathbf{Z}_1 \mathbf{S}_1 \mathbf{Z}_2 \mathbf{S}_2 \mathbf{z} = \mathbf{z}_4^T \mathbf{S}_3^T \mathbf{z}_3 \tag{3.4}$$

Equation (3.4) yields the loop-equation of the four-bar loop in trigonometric form, namely,

$$f(\gamma, \psi; \boldsymbol{\alpha}) = \sin \alpha_2 \sin \alpha_4 \sin \gamma \sin \psi + \cos \alpha_1 \sin \alpha_2 \sin \alpha_4 \cos \gamma \cos \psi$$
$$+ \sin \alpha_1 \sin \alpha_2 \cos \alpha_4 \cos \theta - \sin \alpha_1 \cos \alpha_2 \sin \alpha_4 \cos \psi$$
$$+ \cos \alpha_1 \cos \alpha_2 \cos \alpha_4 - \cos \alpha_3 = 0 \tag{3.5}$$

in which

$$\boldsymbol{\alpha} \equiv [\alpha_1 \ \alpha_2 \ \alpha_3 \ \alpha_4]^T \tag{3.6}$$

Equation (3.5) is the input-output (IO) equation of the four-bar linkage.

3.4. The Five-Bar Loop

Figure 3.5 shows the coordinate axes at each joint, of the five-bar loop. For this loop we also want to end up with a loop-equation in trigonometric form that contains the input and output angles ψ and ϕ only, and no other joint angle of the loop. From Fig. 3.5 we can see that now we have five joints, from which we can eliminate only two by their respective joint rotations, so that the trigonometric form of the loop equation, besides the input and output angles, will contain an extra joint angle. Hence, we chose the loop equation in a form that allows us to eliminate the joint rotations \mathbf{Z}_5 and \mathbf{Z}_9 , and keep the joint rotations \mathbf{Z}_6 and \mathbf{Z}_7 that represent the

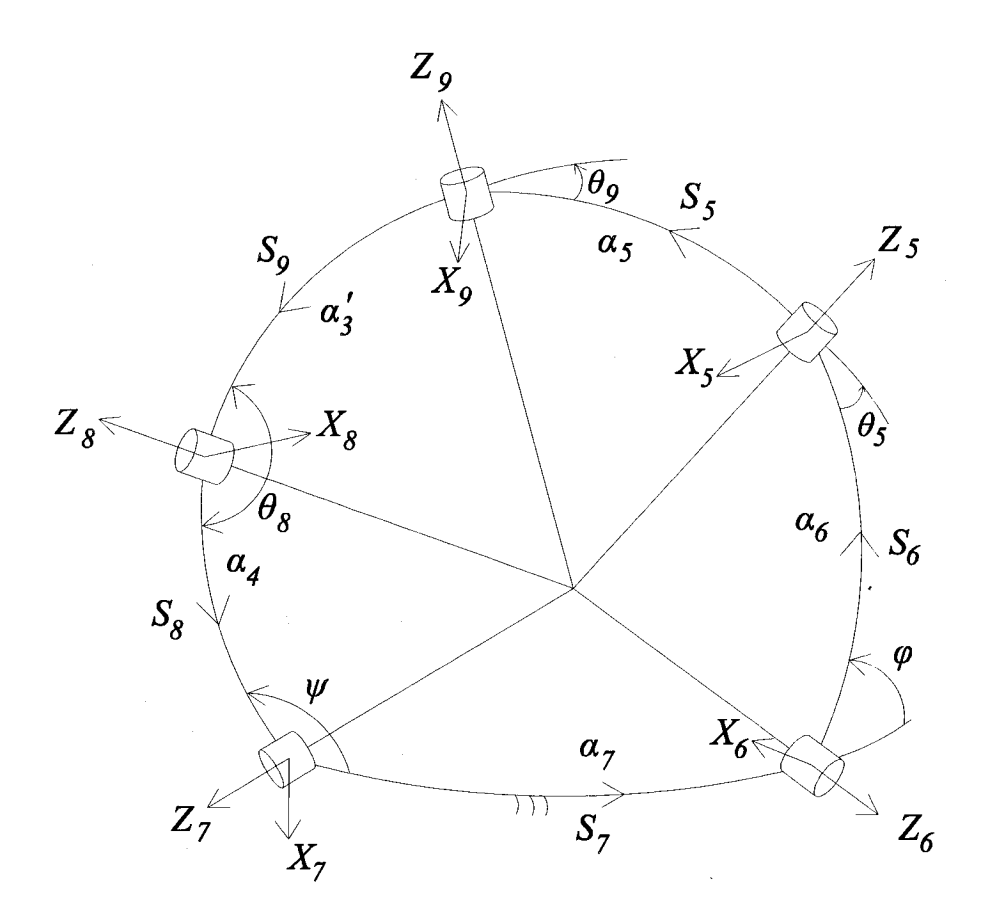


FIGURE 3.5. The five-bar loop

output and input angles as well as the joint rotation \mathbf{Z}_8 ; the latter is common to both the four-bar and the five-bar loops of the spherical Stephenson mechanism.

Thus, the loop-equation that we choose is

$$Z_9S_9Z_8S_8Z_7S_7Z_6S_6Z_5S_5 = 1 (3.7)$$

where

$$\mathbf{Z}_{5} = \begin{bmatrix} \cos heta_{5} & -\sin heta_{5} & 0 \\ \sin heta_{5} & \cos heta_{5} & 0 \\ 0 & 0 & 1 \end{bmatrix}, \quad \mathbf{Z}_{6} = \begin{bmatrix} \cos \phi & -\sin \phi & 0 \\ \sin \phi & \cos \phi & 0 \\ 0 & 0 & 1 \end{bmatrix}$$

$$\mathbf{Z}_{7} = \begin{bmatrix} -\cos\psi & -\sin\psi & 0 \\ \sin\psi & -\cos\psi & 0 \\ 0 & 0 & 1 \end{bmatrix}, \quad \mathbf{Z}_{8} = \begin{bmatrix} -\cos\theta_{8} & -\sin\theta_{8} & 0 \\ \sin\theta_{8} & -\cos\theta_{8} & 0 \\ 0 & 0 & 1 \end{bmatrix}$$
$$\mathbf{Z}_{9} = \begin{bmatrix} \cos\theta_{9} & -\sin\theta_{9} & 0 \\ \sin\theta_{9} & \cos\theta_{9} & 0 \\ 0 & 0 & 1 \end{bmatrix}$$

Matrices \mathbf{Z}_7 and \mathbf{Z}_8 are formulated to involve the internal angles ψ and θ_8 , respectively. Moreover,

$$\mathbf{S}_{5} = \begin{bmatrix} 1 & 0 & 0 \\ 0 & \cos \alpha_{5} & -\sin \alpha_{5} \\ 0 & \sin \alpha_{5} & \cos \alpha_{5} \end{bmatrix}, \quad \mathbf{S}_{6} = \begin{bmatrix} 1 & 0 & 0 \\ 0 & \cos \alpha_{6} & -\sin \alpha_{6} \\ 0 & \sin \alpha_{6} & \cos \alpha_{6} \end{bmatrix}$$
$$\mathbf{S}_{7} = \begin{bmatrix} 1 & 0 & 0 \\ 0 & \cos \alpha_{7} & -\sin \alpha_{7} \\ 0 & \sin \alpha_{7} & \cos \alpha_{4} & -\sin \alpha_{4} \end{bmatrix}$$

$$\mathbf{S}_9 = \left[egin{array}{cccc} 1 & 0 & 0 \\ 0 & \coslpha_3' & -\sinlpha_3' \\ 0 & \sinlpha_3' & \coslpha_3' \end{array}
ight]$$

In order to eliminate the joint rotations \mathbf{Z}_5 and \mathbf{Z}_9 we resort to the relation

$$\mathbf{z}_9^T \mathbf{Z}_9 \mathbf{S}_9 \mathbf{Z}_8 \mathbf{S}_8 \mathbf{Z}_7 \mathbf{S}_7 \mathbf{Z}_6 \mathbf{S}_6 \mathbf{Z}_5 \mathbf{z}_5 = \mathbf{z}_9^T \mathbf{S}_5^T \mathbf{z}_5$$

which simplifies to

$$\mathbf{z}^T \mathbf{S}_9 \mathbf{Z}_8 \mathbf{S}_8 \mathbf{Z}_7 \mathbf{S}_7 \mathbf{Z}_6 \mathbf{S}_6 \mathbf{z} = \mathbf{z}_9^T \mathbf{S}_5^T \mathbf{z}_5 \tag{3.8}$$

Furthermore, to eliminate the undesired angle θ_8 , we express both $\cos \theta_8$ and $\sin \theta_8$ using what is known as the tan-half formulas, namely,

$$\cos \theta_8 = \frac{1 - t_8^2}{1 + t_8^2}, \quad \sin \theta_8 = \frac{2t_8}{1 + t_8^2}, \quad t_8 = \tan(\theta_8/2)$$
 (3.9)

With these substitutions, we define $\bar{\mathbf{Z}}_8$ as

Thus, eq.(3.8) becomes

$$\mathbf{z}^T \mathbf{S}_9 \bar{\mathbf{Z}}_8 \mathbf{S}_8 \mathbf{Z}_7 \mathbf{S}_7 \mathbf{Z}_6 \mathbf{S}_6 \mathbf{z} = \mathbf{z}_9^T \mathbf{S}_5^T \mathbf{z}_5 (1 + t_8^2)$$
(3.10)

Equation (3.10) yields the five-bar loop equation in trigonometric form, namely,

$$g(t_8; \psi, \phi; \tilde{\alpha}) = At_8^2 + Bt_8 + C = 0$$
 (3.11)

where

$$\tilde{\boldsymbol{\alpha}} \equiv [\alpha_3' \ \alpha_4 \ \alpha_5 \ \alpha_6 \ \alpha_7]^T \tag{3.12}$$

$$\begin{split} A(\psi,\phi;\tilde{\boldsymbol{\alpha}}) &= -\sin\alpha_6\sin\phi\sin\psi\sin\alpha_3'\cos\alpha_4 - \cos\alpha_5 - \sin\alpha_6\cos\phi\sin\alpha_7\sin\alpha_3'\sin\alpha_4 \\ &- \sin\alpha_6\cos\phi\cos\alpha_7\cos\psi\sin\alpha_3'\cos\alpha_4 - \sin\alpha_6\cos\phi\sin\alpha_7\cos\alpha_3'\cos\alpha_4 \\ &+ \sin\alpha_6\sin\phi\sin\psi\cos\alpha_3'\sin\alpha_4 + \sin\alpha_6\cos\phi\cos\alpha_7\cos\psi\cos\alpha_3'\sin\alpha_4 \\ &+ \cos\alpha_6\sin\alpha_7\cos\psi\cos\alpha_3'\sin\alpha_4 + \cos\alpha_6\cos\alpha_7\sin\alpha_3'\sin\alpha_4 \\ &+ \cos\alpha_6\cos\alpha_7\cos\alpha_3'\cos\alpha_4 - \cos\alpha_6\sin\alpha_7\cos\psi\sin\alpha_3'\cos\alpha_4 \end{split}$$

3.5. THE IO EQUATION OF THE SPHERICAL STEPHENSON MECHANISM

$$B(\psi, \phi; \tilde{\boldsymbol{\alpha}}) = 2 \sin \alpha_6 \cos \phi \cos \alpha_7 \sin \alpha_3' \sin \psi - 2 \sin \alpha_6 \sin \phi \sin \alpha_3' \cos \psi$$

$$+ 2 \cos \alpha_6 \sin \alpha_7 \sin \alpha_3' \sin \psi$$

$$C(\psi, \phi; \tilde{\boldsymbol{\alpha}}) = -\sin \alpha_6 \cos \phi \sin \alpha_7 \cos \alpha_3' \cos \alpha_4 + \sin \alpha_6 \cos \phi \cos \alpha_7 \cos \psi \cos \alpha_3' \sin \alpha_4$$

$$+ \cos \alpha_6 \sin \alpha_7 \cos \psi \sin \alpha_3' \cos \alpha_4 + \sin \alpha_6 \sin \phi \sin \psi \sin \alpha_3' \cos \alpha_4$$

$$+ \sin \alpha_6 \sin \phi \sin \psi \cos \alpha_3' \sin \alpha_4 + \sin \alpha_6 \cos \phi \sin \alpha_7 \sin \alpha_3' \sin \alpha_4$$

$$- \cos \alpha_6 \cos \alpha_7 \sin \alpha_3' \sin \alpha_4 + \cos \alpha_6 \cos \alpha_7 \cos \alpha_3' \cos \alpha_4$$

$$+ \sin \alpha_6 \cos \phi \cos \alpha_7 \cos \psi \sin \alpha_3' \cos \alpha_4$$

$$+ \sin \alpha_6 \cos \phi \cos \alpha_7 \cos \psi \sin \alpha_3' \cos \alpha_4$$

3.5. The IO Equation of the Spherical Stephenson Mechanism

The subject of this section is the derivation of a single IO equation for the spherical Stephenson mechanism that includes only the input angle ψ and the two output angles γ and ϕ .

We can also have eq.(3.5) as a function of θ_8 . From Fig. 3.1 we notice that $\mu + \beta + \theta_8 = 2\pi$; from the same figure we can find an equation for angle μ , namely,

$$\cos \mu = \frac{\cos \alpha_1 \cos \alpha_2 - \cos \alpha_3 \cos \alpha_4 + \sin \alpha_1 \sin \alpha_2 \cos \gamma}{\sin \alpha_3 \sin \alpha_4}$$
 (3.13)

whence an expression for $\cos \gamma$ is readily derived:

$$\cos \gamma = \frac{\sin \alpha_3 \sin \alpha_4 \cos \mu - \cos \alpha_1 \cos \alpha_2 + \cos \alpha_3 \cos \alpha_4}{\sin \alpha_1 \sin \alpha_2} \tag{3.14}$$

Substituting $\mu = 2\pi - (\beta + \theta_8)$ into eq.(3.14) we have a new expression for $\cos \gamma$, namely,

$$\cos \gamma = \frac{\sin \alpha_3 \sin \alpha_4 (\cos \beta \cos \theta_8 - \sin \beta \sin \theta_8) - \cos \alpha_1 \cos \alpha_2 + \cos \alpha_3 \cos \alpha_4}{\sin \alpha_1 \sin \alpha_2} \quad (3.15)$$

The foregoing expression is now substituted into eq.(3.5), while $\cos \theta_8$ and $\sin \theta_8$ are expressed using the tang-half-angle formulas, eqs.(3.9). Hence the four-bar loop

3.5. THE IO EQUATION OF THE SPHERICAL STEPHENSON MECHANISM equation in trigonometric form is now

$$f(t_8; \psi, \gamma; \alpha, \beta) = Dt_8^2 + Et_8 + F = 0$$
 (3.16)

where

$$D(\psi, \gamma; \boldsymbol{\alpha}, \beta) = \cos \psi \cos \alpha_1 \sin \alpha_3 \cos \beta \cos \alpha_4^2 + \sin \alpha_4 \cos \psi \cos \alpha_1 \cos \alpha_3 \cos \alpha_4$$

$$+ \sin \alpha_2 \sin \alpha_4 \sin \psi \sin \gamma \sin \alpha_1 - \cos \psi \cos \alpha_1 \sin \alpha_3 \cos \beta$$

$$- \cos \alpha_4 \sin \alpha_1 \sin \alpha_3 \sin \alpha_4 \cos \beta + \cos \alpha_4^2 \sin \alpha_1 \cos \alpha_3$$

$$- \cos \alpha_2 \sin \alpha_4 \cos \psi - \cos \alpha_3 \sin \alpha_1$$

$$E(\psi, \gamma; \boldsymbol{\alpha}, \beta) = -2 \cos \psi \cos \alpha_1 \sin \alpha_3 \sin \beta + 2 \cos \psi \cos \alpha_1 \sin \alpha_3 \sin \beta \cos \alpha_4^2$$

$$-2 \cos \alpha_4 \sin \alpha_1 \sin \alpha_3 \sin \alpha_4 \sin \beta$$

$$F(\psi, \gamma; \boldsymbol{\alpha}, \beta) = \cos \psi \cos \alpha_1 \sin \alpha_3 \cos \beta - \cos \psi \cos \alpha_1 \sin \alpha_3 \cos \beta \cos \alpha_4^2$$

$$- \cos \alpha_2 \sin \alpha_4 \cos \psi + \sin \alpha_4 \cos \psi \cos \alpha_1 \cos \alpha_3 \cos \alpha_4$$

$$+ \sin \alpha_2 \sin \alpha_4 \sin \psi \sin \gamma \sin \alpha_1 + \cos \alpha_4^2 \sin \alpha_1 \cos \alpha_3$$

$$- \cos \alpha_3 \sin \alpha_1 + \cos \alpha_4 \sin \alpha_1 \sin \alpha_3 \sin \alpha_4 \cos \beta$$

3.5.1. Elimination Procedure To obtain the IO equation for the spherical Stephenson mechanism, we have to eliminate t_8 from eqs. (3.11 & 3.16). This can be done by means of *dialytic elimination* (Salmon, 1885), as discussed below.

We recall here eqs.(3.11) and (3.16) for quick reference:

$$g(t_8; \psi, \phi; \tilde{\alpha}) = At_8^2 + Bt_8 + C = 0$$
 (3.17a)

$$f(t_8; \psi, \gamma; \alpha, \beta) = Dt_8^2 + Et_8 + F = 0$$
 (3.17b)

In order to eliminate t_8 from the above two equations, we proceed to deriving two additional equations from eqs. (3.17a & b). We do this by multiplying the two sides of each of these equations by t_8 , thereby obtaining a total of four polynomial equations

3.5. THE IO EQUATION OF THE SPHERICAL STEPHENSON MECHANISM in t_8 , namely,

$$At_8^3 + Bt_8^2 + Ct_8 = 0$$
$$Dt_8^3 + Et_8^2 + Ft_8 = 0$$
$$At_8^2 + Bt_8 + C = 0$$
$$Dt_8^2 + Et_8 + F = 0$$

Now we write the above four equations in *linear homogeneous form*, namely,

$$\mathbf{Mt}_8 = \mathbf{0} \tag{3.18}$$

where the 4×4 matrix M and the 4-dimensional vector \mathbf{t}_8 are defined as

$$\mathbf{M} = \left[egin{array}{cccc} A & B & C & 0 \ D & E & F & 0 \ 0 & A & B & C \ 0 & D & E & F \end{array}
ight], \quad \mathbf{t}_8 = \left[egin{array}{c} t_8^3 \ t_8^2 \ t_8 \ \end{array}
ight]$$

From eq.(3.18) it is apparent that a nontrivial solution is possible if and only if M is singular. Hence, the desired IO equation for the spherical Stephenson mechanism is derived from the singularity condition of M, i.e.,

$$q(\psi, \gamma, \phi; \hat{\boldsymbol{\alpha}}, \beta) = \det(\mathbf{M}) = 0 \tag{3.19}$$

with,

$$\hat{\boldsymbol{\alpha}} \equiv [\alpha_1 \ \alpha_2 \ \alpha_3 \ \alpha_3' \ \alpha_4 \ \alpha_5 \ \alpha_6 \ \alpha_7]^T \tag{3.20}$$

$$\det(\mathbf{M}) = AEBF - ACE^2 - A^2F^2 + 2ADFC - DB^2F + DBCE - D^2C^2 \quad (3.21)$$

3.6. Dimensional Synthesis of the Spherical Stephenson Mechanism

Equation (3.19) expresses the relationship among all link dimensions and the angles ψ , γ and ϕ , with ψ as the input, the others as output. This equation can be used for either the analysis of the spherical Stephenson mechanism with a given set of linkage dimensions or its dimensional synthesis.

To synthesize the spherical Stephenson mechanism, we define first the design vector \mathbf{y} as

$$\mathbf{y} = [\alpha_1 \ \alpha_2 \ \alpha_3 \ \alpha_3' \ \alpha_4 \ \alpha_5 \ \alpha_6 \ \alpha_7 \ \beta]^T \tag{3.22}$$

If the desired motion of a spherical Stephenson mechanism is specified by m input-output triads $\{\psi_i, \gamma_i, \phi_i\}_{i=1}^m$, with m > 9, the dimension of \mathbf{y} , then a problem of approximate synthesis is formulated.

Substituting $\{\psi_i, \gamma_i, \phi_i\}_{i=1}^m$ into eq.(3.19), we obtain

$$q_i = q(\mathbf{d}_i; \mathbf{y}) = \det(\mathbf{M}_i) = 0 \tag{3.23}$$

where $\mathbf{d}_i = [\psi_i \ \gamma_i \ \phi_i]^T$, for $i = 1, \dots, m$, and \mathbf{M}_i is a function of the *i*th input-output triad.

For the input-output triads we change the location of the zeros to consider in the synthesis the initial position of the mechanism. To this end, we rewrite the input and output angles in an incremental form, in terms of $\{\Delta\psi_i, \Delta\gamma_i, \Delta\phi_i\}_{i=1}^m$, i.e.,

$$\psi_i = \psi_0 + \Delta \psi_i$$
$$\gamma_i = \gamma_0 + \Delta \gamma_i$$
$$\phi_i = \phi_0 + \Delta \phi_i$$

3.6. DIMENSIONAL SYNTHESIS OF THE SPHERICAL STEPHENSON MECHANISM

where ψ_0 , γ_0 and ϕ_0 are the reference angles that are now grouped in an 12-dimensional design vector $\bar{\mathbf{y}}$:

$$\bar{\mathbf{y}} = [\alpha_1 \ \alpha_2 \ \alpha_3 \ \alpha_3' \ \alpha_4 \ \alpha_5 \ \alpha_6 \ \alpha_7 \ \beta \ \psi_0 \ \phi_0 \ \gamma_0]^T$$

Then, eq.(3.19) takes the form

$$q(\Delta \mathbf{d}_i; \bar{\mathbf{y}}) = 0$$

where

$$\Delta \mathbf{d}_i = [\Delta \psi_i \ \Delta \gamma_i \ \Delta \phi_i]^T, \quad i = 1, \dots, m$$

Using the tan-half formulas, let

$$x_i = \tan(\alpha_i/2), \quad i = 1, \dots, 7$$
 (3.24a)

$$x_8 = \tan(\alpha_3'/2) \tag{3.24b}$$

$$x_9 = \tan(\beta/2) \tag{3.24c}$$

$$x_{10} = \tan(\psi_0/2) \tag{3.24d}$$

$$x_{11} = \tan(\gamma_0/2) \tag{3.24e}$$

$$x_{12} = \tan(\phi_0/2) \tag{3.24f}$$

and

$$\cos \alpha_i = \frac{1 - x_i^2}{1 + x_i^2}$$
, $\sin \alpha_i = \frac{2x_i}{1 + x_i^2}$, $i = 1...7$ (3.25a)

$$\cos \alpha_3' = \frac{1 - x_8^2}{1 + x_8^2} \quad , \quad \sin \alpha_3' = \frac{2x_8}{1 + x_8^2}$$
 (3.25b)

$$\cos \beta = \frac{1 - x_9^2}{1 + x_9^2} \quad , \quad \sin \beta = \frac{2x_9}{1 + x_9^2}$$
 (3.25c)

$$\cos \psi_0 = \frac{1 - x_{10}^2}{1 + x_{10}^2} \quad , \quad \sin \psi_0 = \frac{2x_{10}}{1 + x_{10}^2} \tag{3.25d}$$

$$\cos \gamma_0 = \frac{1 - x_{11}^2}{1 + x_{11}^2} \quad , \quad \sin \gamma_0 = \frac{2x_{11}}{1 + x_{11}^2} \tag{3.25e}$$

$$\cos \phi_0 = \frac{1 - x_{12}^2}{1 + x_{12}^2} \quad , \quad \sin \phi_0 = \frac{2x_{12}}{1 + x_{12}^2} \tag{3.25f}$$

3.6. DIMENSIONAL SYNTHESIS OF THE SPHERICAL STEPHENSON MECHANISM thereby defining a system of m > 12 nonlinear equations in 12 unknowns, namely,

$$q(x) = 0$$

where $\mathbf{x} = [x_1, \dots, x_{12}]^T$. This is an overdetermined system of nonlinear equations whose least square approximation yields the optimum linkage sought. The associated unconstrained nonlinear least-square problem is thus

$$z(\mathbf{x}) = \frac{1}{2} \mathbf{q}^T \mathbf{W} \mathbf{q} \to \min_{\mathbf{x}}$$

where **W** is an $m \times m$ positive-definite weighting matrix. When all the m nonlinear equations of vector **q** are considered with the same weight, the weighting matrix **W** can be defined as a multiple of the $m \times m$ identity matrix, namely,

$$\mathbf{W} = \frac{1}{m} \mathbf{1}$$

In order to reduce vibrations, the input link and the two output links should be capable of a full rotation. We define first the pairs of angles $\{\psi_i, \gamma_i\}_{i=1}^m$ from the corresponding four-bar linkage with input and output cranks. Below we explain how this linkage is found.

3.6.1. Spherical Drag-Link Mechanism We need a four-bar spherical linkage of the drag-link type, i.e., of the crank-crank type, with a good *transmission quality*, i.e., a good force transmission by avoiding large absolute values of the cosine of the transmission angle (Angeles and Bernier, 1987).

For the design of this spherical drag-link mechanism we resort to the concept of zero-mean linkages, as proposed by Zanganeh and Angeles (1994). This concept is described in the subsection below.

Zero-Mean Linkages. From Fig. 3.6 and eq.(3.5), the IO equation of the spherical four-bar linkage, expressed in terms of *Freudenstein parameters* is written as

$$f(\delta, \sigma, \mathbf{k}) = k_1 - k_2 \cos \sigma + k_3 \cos \delta + k_4 \cos \delta \cos \sigma + \sin \delta \sin \sigma = 0$$
 (3.26)

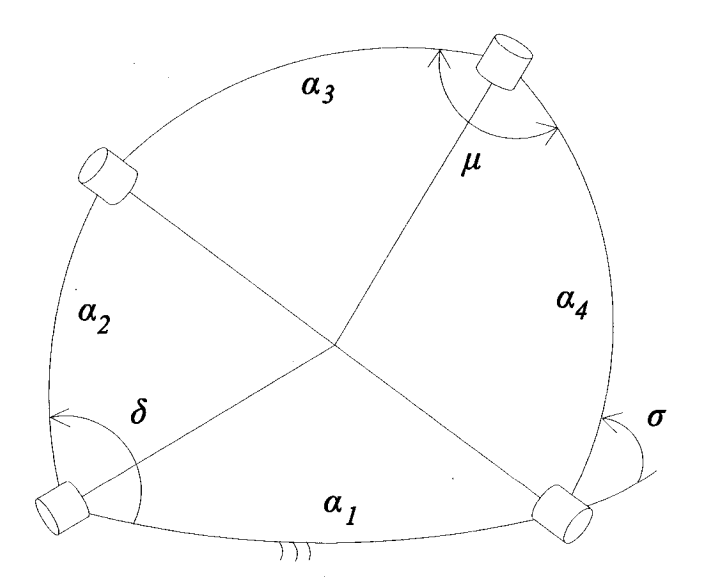


FIGURE 3.6. The 4 bar mechanism

where $\mathbf{k} = [k_1, k_2, k_3, k_4]^T$ is the Freudenstein-parameter vector, with the definitions below:

$$k_1 = \frac{\cos \alpha_1 \cos \alpha_2 \cos \alpha_4 - \cos \alpha_3}{\sin \alpha_2 \sin \alpha_4} \tag{3.27a}$$

$$k_{1} = \frac{\cos \alpha_{1} \cos \alpha_{2} \cos \alpha_{4} - \cos \alpha_{3}}{\sin \alpha_{2} \sin \alpha_{4}}$$

$$k_{2} = \frac{\sin \alpha_{1} \cos \alpha_{2}}{\sin \alpha_{2}}$$
(3.27a)
$$(3.27b)$$

$$k_3 = \frac{\sin \alpha_1 \cos \alpha_4}{\sin \alpha_4} \tag{3.27c}$$

$$k_4 = \cos \alpha_1 \tag{3.27d}$$

For this mechanism, the cosine of the transmission angle μ is given by

$$\cos \mu = \frac{\cos \alpha_1 \cos \alpha_2 - \cos \alpha_3 \cos \alpha_4 + \sin \alpha_1 \sin \alpha_2 \cos \delta}{\sin \alpha_3 \sin \alpha_4}$$
 (3.28)

As introduced in (Gosselin and Angeles, 1989) the transmission quality of a fourbar mechanism is

$$Q = \frac{1}{2\pi} \int_0^{2\pi} \sin^2 \mu \, d\delta \tag{3.29}$$

3.6. DIMENSIONAL SYNTHESIS OF THE SPHERICAL STEPHENSON MECHANISM

its complement being the transmission defect, defined as:

$$D = \frac{1}{2\pi} \int_0^{2\pi} \cos^2 \mu \, d\delta \tag{3.30}$$

Hence,

$$Q + D = 1$$

It is apparent that the transmission quality is maximized if the transmission defect is minimized.

From eq.(3.28) the cosine of the transmission angle can be written as

$$\cos \mu = c_1 + c_2 \cos \delta \tag{3.31}$$

where

$$c_1 = \frac{\cos \alpha_1 \cos \alpha_2 - \cos \alpha_3 \cos \alpha_4}{\sin \alpha_3 \sin \alpha_4} \tag{3.32a}$$

$$c_{1} = \frac{\cos \alpha_{1} \cos \alpha_{2} - \cos \alpha_{3} \cos \alpha_{4}}{\sin \alpha_{3} \sin \alpha_{4}}$$

$$c_{2} = \frac{\sin \alpha_{1} \sin \alpha_{2}}{\sin \alpha_{3} \sin \alpha_{4}}$$
(3.32a)
$$(3.32b)$$

Thus, D becomes, for an input crank,

$$D = c_1^2 + \frac{1}{2}c_2^2 \tag{3.33}$$

where c_1^2 and c_2^2 are positive-semidefinite and positive-definite quantities, respectively, i.e.,

$$c_1^2 \ge 0, \quad c_2^2 > 0$$

Thus, the second term of the right-hand side of eq. (3.33) cannot vanish, whereas the first one can. This leads to the definition of a specific class of linkages, called zero-mean linkages, for which $c_1 = 0$. From eq.(3.31) it is apparent that c_1 and $1/2 c_2^2$ are, in fact, the expected value and the variance of the cosine of the transmission 3.6. DIMENSIONAL SYNTHESIS OF THE SPHERICAL STEPHENSON MECHANISM angle i.e.,

$$c_1 = E(\cos \mu); \quad \frac{1}{2}c_2^2 = Var(\cos \mu)$$

When substituting $\cos \alpha_i$ and $\sin \alpha_i$ in terms of the Freudenstein parameters k_i , for i = 1, ..., 4, in eq.(3.32a), with c_1 equated to zero, we obtain

$$k_2k_4 + k_1k_3 = 0 (3.34)$$

as the *zero-mean* condition for spherical four-bar linkages (Gosselin and Angeles, 1989).

The expression for D under the zero-mean condition becomes

$$D = \frac{1}{2}c_2^2 = \frac{(1-\tau)\lambda}{4(1+k_2^2-k_1^2)}$$
 (3.35)

where

$$\tau = [k_2 k_3 k_4 - k_1 (1 - k_4^2)] [1 + k_2^2 - k_4^2) \lambda]^{1/2}$$

$$\lambda = 1 + k_3^2 - k_4^2$$

Mobility Conditions. The general mobility conditions for a spherical four-bar linkage (Zanganeh and Angeles, 1994) for the input link are in terms of the Freudestein parameters,

$$(k_3 + k_1)^2 \le (k_4 - k_2)^2 \tag{3.36a}$$

$$(k_3 - k_1)^2 \le (k_4 + k_2)^2 \tag{3.36b}$$

The corresponding conditions for the output link are

$$(k_1 - k_2)^2 \le (k_3 + k_4)^2 \tag{3.36c}$$

$$(k_1 + k_2)^2 \le (k_3 + k_4)^2 \tag{3.36d}$$

For drag-link spherical linkages the inequalities (3.36a–d) must be satisfied simultaneously. Thus, using the zero-mean condition, the general mobility conditions can be simplified as (Zanganeh and Angeles, 1994)

$$k_2^2 \le k_1^2 \tag{3.37a}$$

$$k_3^2 \le k_4^2$$
 (3.37b)

$$k_1^2 \le k_4^2$$
 (3.37c)

$$k_4^2 \le 1$$
 (3.37d)

Constrained Optimization with Arbitrary Objective Function. The software library ODA, developed by ChinPun Teng in 1999 at McGill University, was used to obtain the optimum design of the spherical drag-link mechanism. This library is based on the *Orthogonal-Decomposition Algorithm* (Teng and Angeles, 2001). ODA can handle several classes of optimization problems, such as unconstrained linear least-square problems (over-, under-, or determined system of equations), constrained linear least-square problems, unconstrained nonlinear least-square problems, constrained nonlinear least-square problems, and constrained problems with an arbitrary objective function. In our case, we formulate the problem as

$$z = D(\mathbf{k}) \to \min_{\mathbf{k}}$$

subject the nonlinear equality constraints of eq.(3.34) and the nonlinear inequality constraints of eqs.(3.37a-d). The latter were converted to equality constraints by

3.6. DIMENSIONAL SYNTHESIS OF THE SPHERICAL STEPHENSON MECHANISM means of slack variables $\{s_i\}_{1}^{3}$, taking the vector \mathbf{k} of Freudestein parameters as the design vector.

Notice that due to the features of our design, we already know the value $\alpha_1 = 135^{\circ}$, which yields k_4 from eq.(3.27d). This value was substituted in our formulation, thus reducing the dimension of the design vector by one and eliminating the nonlinear inequality constraint (3.37d).

The problem is now formulated as an equality-constrained optimization problem, namely,

$$z = D(\mathbf{x}) \to \min_{\mathbf{x}}$$

subject to

$$g_1(\mathbf{x}) = k_2 k_4 + k_1 k_3 = 0 \tag{3.38a}$$

$$g_2(\mathbf{x}) = k_1^2 - k_4^2 + s_1^2 = 0$$
 (3.38b)

$$g_3(\mathbf{x}) = k_2^2 - k_1^2 + s_2^2 = 0$$
 (3.38c)

$$g_4(\mathbf{x}) = k_3^2 - k_4^2 + s_3^2 = 0 (3.38d)$$

In this formulation, the design vector is redifined as

$$\mathbf{x} = [k_1 \ k_2 \ k_3 \ s_1 \ s_2 \ s_3]^T$$

but only the Freudestein parameters occur in z(x).

The solution obtained by the ODA package is

$$z_{min} = 0.124764, \quad \mathbf{x} = [-0.007829 \ 0.000125 \ 0.002269]^T$$
 (3.39)

with $s_1 = 0.707634$, $s_2 = -0.007828$ and $s_3 = 0.707063$.

3.6. DIMENSIONAL SYNTHESIS OF THE SPHERICAL STEPHENSON MECHANISM

From eq.(3.39) we can see that the minimum linkage defect is about 12.48%; hence, the mechanism has a transmission quality of 87.52%, which is acceptable². A transmission quality of 100% is unreachable because the transmission angle μ changes as the input angle changes.

Substituting the foregoing optimum values of the Freudestein parameters, with $k_4 = -0.707107$, into eq.(3.27b-d) and solving for the link dimensions, we have:

$$\alpha_1 = 135^{\circ}, \quad \alpha_2 = 89.99^{\circ}, \quad \alpha_3 = 89.55^{\circ}, \quad \alpha_4 = 89.82^{\circ}$$

These values are close to those of the universal joint (UJ), whose link dimensions α_2 , α_3 and α_4 take the value of 90°, with input and output axes at an angle of 45° $(180^{\circ} - \alpha_1)$.

Figure 3.7 shows the plots of the output angle σ vs. the input angle δ of the main mechanism and its conjugate. From the same figure we can see that the input and output links are cranks.

Figure 3.8 shows the plot of the transmission angle μ vs. the input angle δ of the main mechanism. We can see from this figure that the maximum and minimum values of the transmission angle are 135° and 45°, respectively, these two values being the sugested maximum and minimum allowed values of the transmission angle of a four-bar linkage (Norton, 2001). The average of the transmission angle μ of the universal joint with input and output shaft axes at an angle of 45° is 90°, which is the desired value for a good transmission quality.

At this point, we can conclude that the foregoing universal joint garantees both a full rotation of the input and output angles and a good transmission quality, for the given value of angle between input and output shaft axes.

²Of course, what is acceptable is subjective. As a guideline, we looked at McGill University's marking scheme, under which the highest grade is A, that corresponds to a student's performance ranging from 85% to 100%.

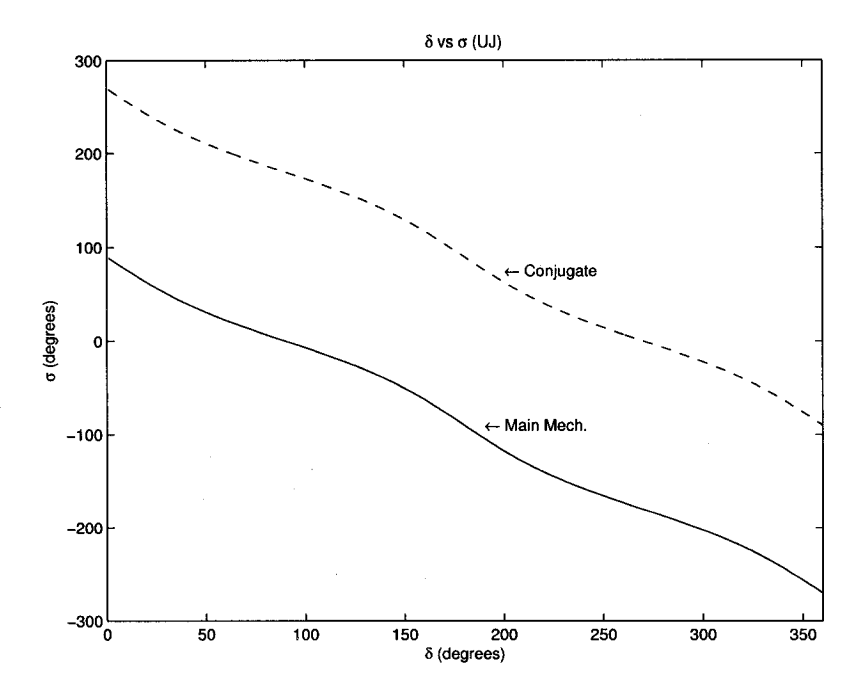


FIGURE 3.7. σ vs. δ for the main mechanism and its conjugate

3.6.2. Optimum Synthesis of the Spherical Stephenson Mechanism In our design we have the freedom to choose any IO function with the sole condition that the input and output links be cranks. According to the linkage configurations shown in Figs. 3.1 and 3.6, we make the pairs $\{\psi_i, \gamma_i\}_{i=1}^m$ equal to the pairs $\{\sigma_i, \delta_i\}_{i=1}^m$ of the universal joint. In order to form the IO triads $\{\psi_i, \gamma_i, \phi_i\}_{i=1}^m$ of the mechanism under synthesis we make the set $\{\phi_i\}_{i=1}^m$ equal to $\{\delta_i\}_{i=1}^m$ because this set corresponds to a drag-link mechanism. Hence,

$$\{\psi_i, \gamma_i, \phi_i\}_{i=1}^m = \{\sigma_i, \delta_i, \delta_i\}_{i=1}^m$$

Changing the zeros of the Input and Outputs Triads. We can take m = 360 in order to produce 360 triads $\{\psi_i, \gamma_i, \phi_i\}_{i=1}^{360}$, then substitute them into eq.(3.19) to generate a vector \mathbf{q} of dimension 360, whose *i*th component is $F(\psi_i, \gamma_i, \phi_i, \boldsymbol{\alpha}, \boldsymbol{\beta})$. It is also convenient to allow for the optimum location of the zeros of the input and output triads (Liu and Angeles, 1993). This can be done if we regard the original IO pairs as a set of input and output angle increments $\{\Delta\psi_i, \Delta\gamma_i, \Delta\phi_i\}_{i=1}^{360}$. If ψ_0, γ_0 and

3.6. DIMENSIONAL SYNTHESIS OF THE SPHERICAL STEPHENSON MECHANISM ϕ_0 represent the location of the zeros of the three foregoing angles, we then have

$$\psi_i = \psi_0 + \Delta \psi_i, \quad \gamma_i = \gamma_0 + \Delta \gamma_i, \quad \phi_i = \phi_0 + \Delta \phi_i$$

Geometrically, this means that we move all the points of the set $\{\psi_i, \gamma_i, \phi_i\}_{i=1}^{360}$ to an optimum relocation under a pure translation in the ψ - γ - ϕ space, given by the values ψ_0 , γ_0 and ϕ_0 . Then, eq.(3.19) takes the form

$$F(\psi_0 + \Delta\psi_i, \, \gamma_0 + \Delta\gamma_i, \, \phi_0 + \Delta\phi_i, \, \hat{\boldsymbol{\alpha}}, \, \beta) = \det(\mathbf{M}) = 0$$
 (3.40)

Thus, from the above equation, we can formulate the synthesis problem at hand as an unconstrained nonlinear least-square optimization problem.

Unconstrained Nonlinear Least-Square Problem. The synthesis problem is defined as: Find an aproximate solution to the overdeterminated system of nonlinear equations

$$q(x) = 0$$

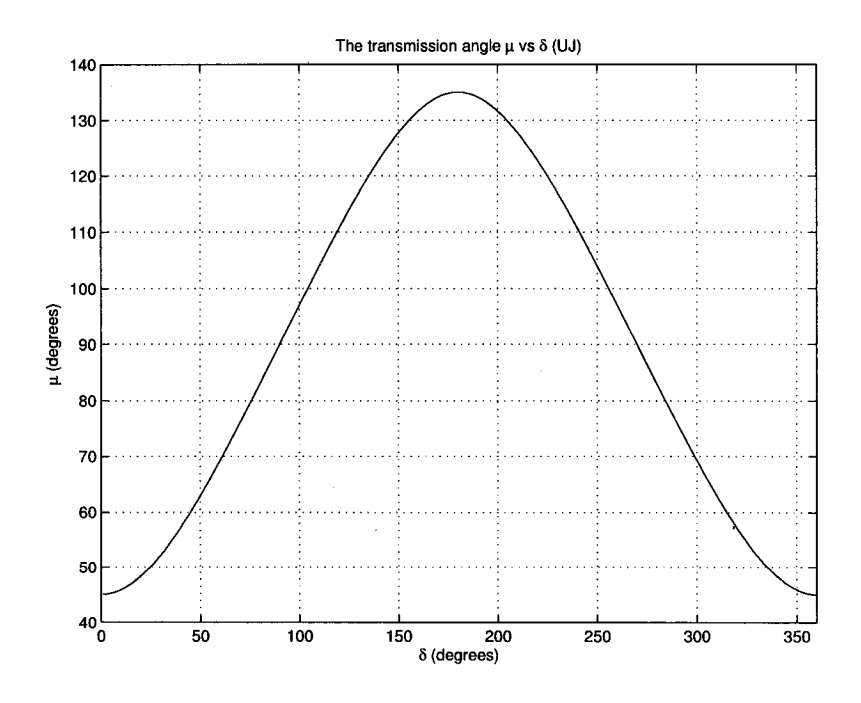


FIGURE 3.8. The transmission angle μ vs δ .

3.6. DIMENSIONAL SYNTHESIS OF THE SPHERICAL STEPHENSON MECHANISM

with the least-square error, where \mathbf{q} and \mathbf{x} are m- and n-dimensional vectors, respectively, with m > n. The problem is described as

$$z(\mathbf{x}) = \frac{1}{2} \mathbf{q}^T \mathbf{W} \mathbf{q} \to \min_{\mathbf{x}}$$

with **W** defined as an $m \times m$ positive-definite weighting matrix, to be determined according to problem needs.

From the features of our design, as explained in Chapter 1, we know that both α_1 and α_7 are equal to 135°. These values are substituted into eq.(3.40); for the remaining link dimensions, their *cosine* and *sine* function are then expressed in terms of tan-half angle formulas, as shown below

$$\cos \alpha_{i+1} = \frac{1 - x_i^2}{1 + x_i^2} \quad , \quad \sin \alpha_{i+1} = \frac{2x_i}{1 + x_i^2}, \quad i = 1, 2$$
 (3.41a)

$$\cos \alpha_3' = \frac{1 - x_3^2}{1 + x_3^2} \quad , \quad \sin \alpha_3' = \frac{2x_3}{1 + x_3^2}$$
 (3.41b)

$$\cos \alpha_i = \frac{1 - x_i^2}{1 + x_i^2}$$
, $\sin \alpha_i = \frac{2x_i}{1 + x_i^2}$, $i = 4, 5, 6$ (3.41c)

$$\cos \beta = \frac{1 - x_7^2}{1 + x_7^2} \quad , \quad \sin \beta = \frac{2x_7}{1 + x_7^2}$$
 (3.41d)

The angles ψ_0 , γ_0 and ϕ_0 , are also expressed in terms of the tan-half angle formulas, namely,

$$\cos \psi_0 = \frac{1 - x_8^2}{1 + x_8^2} \quad , \quad \sin \psi_0 = \frac{2x_8}{1 + x_8^2}$$
 (3.41e)

$$\cos \gamma_0 = \frac{1 - x_9^2}{1 + x_9^2} \quad , \quad \sin \gamma_0 = \frac{2x_9}{1 + x_9^2}$$
 (3.41f)

$$\cos \phi_0 = \frac{1 - x_{10}^2}{1 + x_{10}^2} \quad , \quad \sin \phi_0 = \frac{2x_{10}}{1 + x_{10}^2} \tag{3.41g}$$

Thus, the design vector \mathbf{x} is 10-dimensional.

Therefore, substituing eqs. (3.41a-g) into eq. (3.40), vector \mathbf{q} is now expressed as a function of the design vector \mathbf{x} of the input and output angle increments, as shown

3.6. DIMENSIONAL SYNTHESIS OF THE SPHERICAL STEPHENSON MECHANISM below:

$$\mathbf{q}(\mathbf{x}; \Delta \psi_i, \Delta \gamma_i, \Delta \phi_i) = \mathbf{0}; \quad i = 1 \dots 360$$

Thus, the unconstrained nonlinear least-square problem is

$$z_2(\mathbf{x}) = \frac{1}{2} \mathbf{q}^T \mathbf{W} \mathbf{q} \to \min_{\mathbf{x}}$$
 (3.42)

If all the 360 components of vector \mathbf{q} were considered with the same weight, the weighting matrix \mathbf{W} is defined as a multiple of the 360×360 identity matrix. Moreover, if that multiple is given by 1/m, where m is the dimension of the design vector, then z_2 is half the square of the rms error of the approximation of the m nonlinear equations. In our case, m = 360.

The numerical solution obtained is

 $\mathbf{x}_{opt} = \begin{bmatrix} 0.6814 \ 0.8022 \ 0.0181 \ 0.8934 \ 0.8036 \ 0.9555 \ 0.2313 \ 0.0658 \ 0.0652 \ 0.0243 \end{bmatrix}^T$ which yields $e_{rms} = 2.24 \times 10^{-6}$.

Substituing \mathbf{x}_{opt} into eqs.(3.41a..d) we obtain the link dimensions of the mechanism, namely,

α_1	$lpha_2$	α_3	$lpha_3'$	$lpha_4$	$lpha_5$	$lpha_6$	$lpha_7$	β
135°	68.54°	77.48°	2.07°	83.55°	77.57°	87.39°	135°	26.05°

while the locations of the zeros of the input and output angles are

ψ_0	γ_0	ϕ_0			
7.53°	7.46°	2.78°			

From the link dimensions we can see that the value of α'_3 is too small to be practical. We can increase this value by forcing α'_3 to be close to 90°. This is done by adjoining

$$\cos \alpha_3' = \frac{1 - x_3^2}{1 + x_3^2} = 0$$

or

$$1 - x_3^2 = 0 (3.43)$$

to the components of vector \mathbf{q} . The dimension of \mathbf{q} being now 361. Thus, the 361st component of \mathbf{q} is

$$q_{361} = 1 - x_3^2$$

We formulated the new optimization problem as an unconstrained weighted non-linear least-square problem, taking the weighting matrix \mathbf{W} as a 361 \times 361 diagonal matrix, namely,

$$\mathbf{W} = diag(w_1, w_2, \dots, w_{360}, w_{361})$$

for normalized weights w_i obeying

$$\sum_{i=1}^{361} w_i = 1 \tag{3.44}$$

The new optimization problem is thus

$$z_3(\mathbf{x}) = \frac{1}{2} \mathbf{q}^T \mathbf{W} \mathbf{q} \to \min_{\mathbf{x}}$$
 (3.45)

Taking into account eq.(3.44) for the numerical solution, we assign the same weight to the first 360 equations, and a different weight to the 361st equation.

Table 3.1 shows the optimum solution for different weights chosen.

From Table 3.1 we can see that the numerical solution with the minimum e_{rms} found was for

$$w_1 = w_2 = \dots = w_{360} = \frac{0.9}{360}; \quad w_{361} = 0.1$$

with

$$e_{rms} = 1.32 \times 10^{-5}$$

For the these weights, the link dimensions are

$lpha_1$	$lpha_2$	$lpha_3$	$lpha_3'$	$lpha_4$	$lpha_5$	$lpha_6$	$lpha_7$	β
135°	84.75°	70.25°	88.99°	86.08°	76.99°	83.23°	135°	56.85°

3.6. DIMENSIONAL SYNTHESIS OF THE SPHERICAL STEPHENSON MECHANISM

Weights	$lpha_2$	α_3	$lpha_3'$	$lpha_4$	$lpha_5$	$lpha_6$	β	e_{rms}
$w_i = 0.9/360$			-					
$w_{361} = 0.1$	84.75°	70.25°	88.99°	86.08°	76.99°	83.23°	56.85°	1.32×10^{-5}
$w_i = 0.8/360$								
$w_{361} = 0.2$	85.32°	70.85°	89.19°	87.24°	76.56°	83.81°	59.62°	2.14×10^{-4}
$w_i = 0.7/360$								
$w_{361} = 0.3$	85.25°	70.72°	89.50°	87.27°	76.51°	83.69°	59.37°	3.22×10^{-4}
$w_i = 0.6/360$								
$w_{361} = 0.4$	86.29°	71.78°	89.99°	90.63°	74.85°	84.46°	64.90°	3.14×10^{-4}
$w_i = 0.5/360$								
$w_{361} = 0.5$	85.98°	70.84°	89.99°	90.51°	74.68°	83.91°	63.53°	1.89×10^{-4}
$w_i = 0.4/360$								·
$w_{361} = 0.6$	85.67°	71.12°	89.99°	90.27°	75.16°	84.17°	63.16°	4.91×10^{-4}
$w_i = 0.3/360$								
$w_{361} = 0.7$	84.82°	70.19°	90°	89.27°	74.42°	87.26°	61.86°	5.67×10^{-3}
$w_i = 0.2/360$								-
$w_{361} = 0.8$	85.08°	70.32°	90°	90°	75.33°	83.55°	61.32°	7.25×10^{-3}
$w_i = 0.1/360$								
$w_{361} = 0.9$	85.06°	71.71°	90°	89.06°	76.48°	87.09°	64.23°	6.68×10^{-3}

TABLE 3.1. Numerical results of the weighted nonlinear least-square optimization

CHAPTER 4

Design Embodiment

The synthesized dimensions were adjusted to values that are practical to avoid large manufacturing errors. Table 4.1 shows both the synthesized and the adjusted dimensions of the spherical Stephenson mechanism.

We validate these results using PRO/ENGINEER, a CAD software package for mechanical design and analysis, and its module PRO/MECHANICA, that provides motion analysis, simulation and animation of complex mechanisms.

4.1. Input-Output Relations

It is noted that the change from the synthesized dimensions to the adjusted dimensions should affect the motion of the mechanism. Fig. 4.1 shows that there is a small difference between the output angles of the synthesized and adjusted mechanisms.

Mechanism	α_1	$lpha_2$	α_3	$lpha_3'$	α_4	α_5	$lpha_6$	α_7	β
Synthesized	135°	84.75°	70.25°	88.99°	86.08°	76.99°	83.23°	135°	56.85°
Adjusted	135°	85°	70°	90°	85°	75°	85°	135°	55°

Table 4.1. Synthesized and adjusted dimensions of the spherical Stephenson mechanism

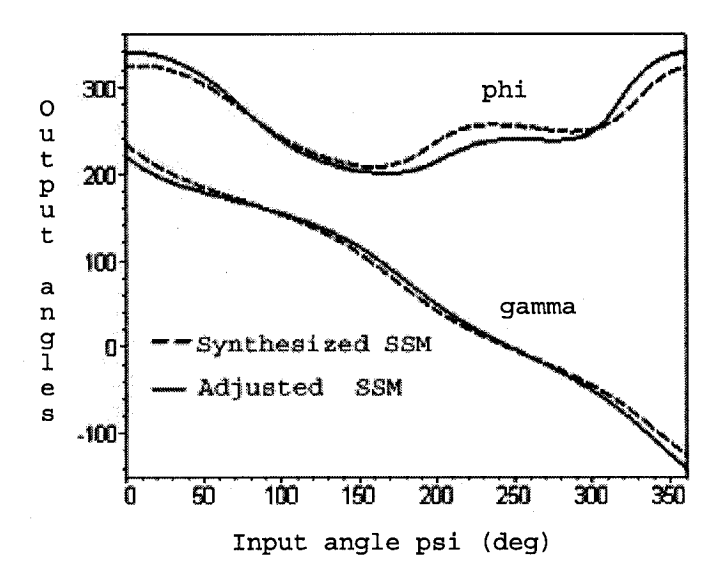


FIGURE 4.1. Output angles vs. ψ of the synthesized and adjusted mechanisms

From Fig. 4.1 we can see that the angles γ and ψ attain values corresponding to full mobility of the input and output links of the four-bar loop for the optimum values of α_2 and α_4 , as required. However, from the same Figure, the plot of the output angle ϕ , shows that the corresponding link α_6 works as a rocker, with mobility within the interval [205°, 318°].

In the optimization problem we expected a full rotatability of the above-mentioned output link, but we did not impose any constraint on full rotatability. We could not find such constraint in the literature and neither the rotatability of Spherical Stephenson mechanisms nor that of spherical five-bar linkages. The only information that we have are theorems and corollaries of rotatability criteria of spherical five-bar linkages, as reported by Kolhi and Khonji (1994).

We adopted the rocker output as a solution because it can also transmit the motion from the main mechanism to its mirror image without changing the kinematics of the whole system. The spherical Stephenson mechanism with the adjusted link dimensions is of the crank-crank-rocker type.

4.2. Transmission Angles

Figures 4.2 and 4.3 show the plot of the transmission angles η and ν , respectively, of the Stephenson mechanism of Fig. 3.1. Angle η attains the maximum value of 148.23° and a minimum of 49.1°, with an average of 98.66°. Angle ν attains a maximum value of 122.36° and a minimum of 37.89°, with an average of 80.12°. This implies a deadlock-free transmission and a good transmission quality.

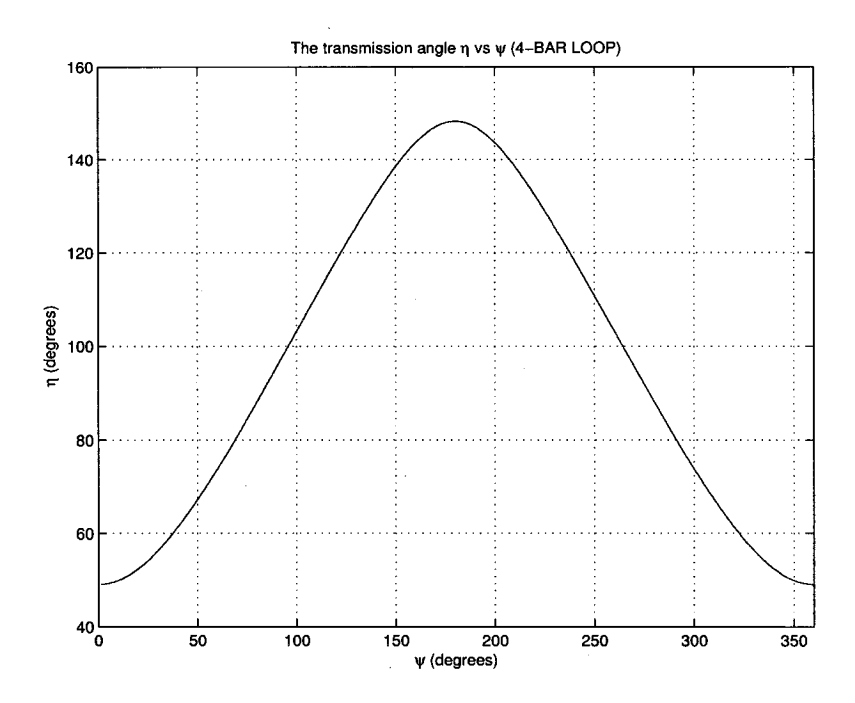


FIGURE 4.2. Transmission angle η vs. ψ

4.3. The Virtual Prototype

Figure 4.4 shows the kinematic chain of the Stephenson mechanism, whose coupler is a ternary link with the shape of a spherical triangle. This chain should be embodied in such a way that interferences be avoided, while attending manufacturability and

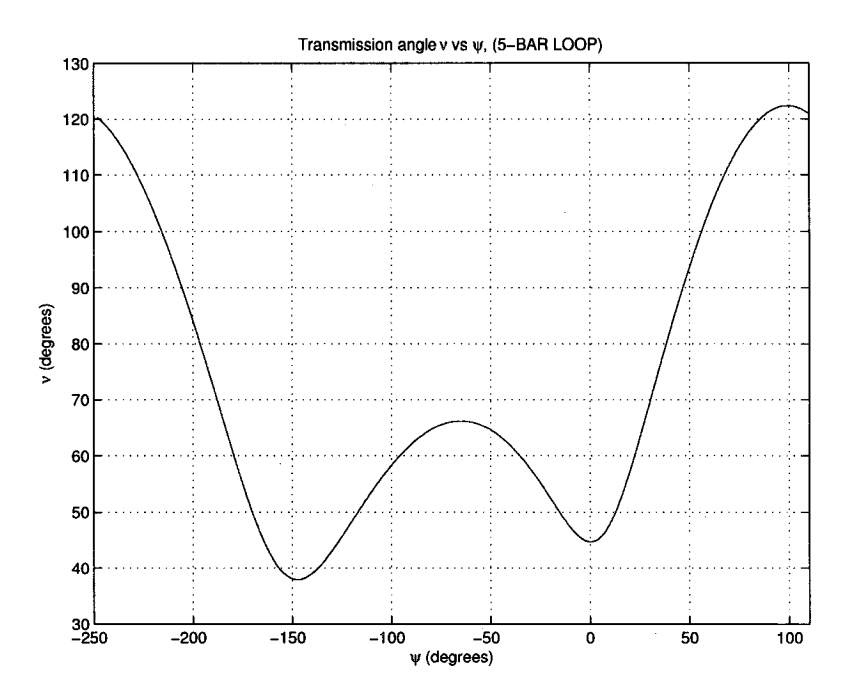


FIGURE 4.3. Transmission angle ν vs. ψ

assemblability issues; for this reason, we shaped the coupler in a convinient form, thereby obtaining the preliminary embodiment shown in Fig. 4.5.

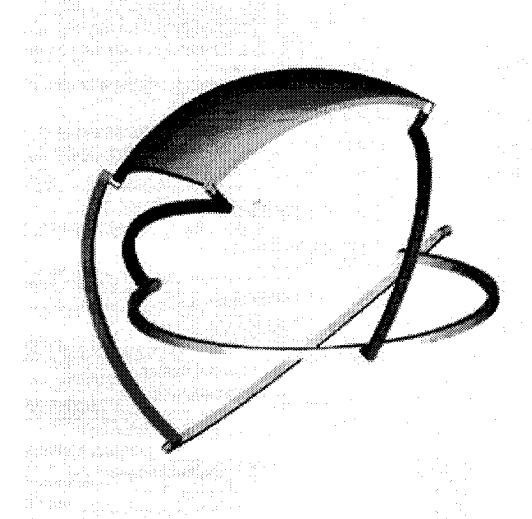


FIGURE 4.4. Rendering of the kinematic chain of the optimum spherical Stephenson mechanism

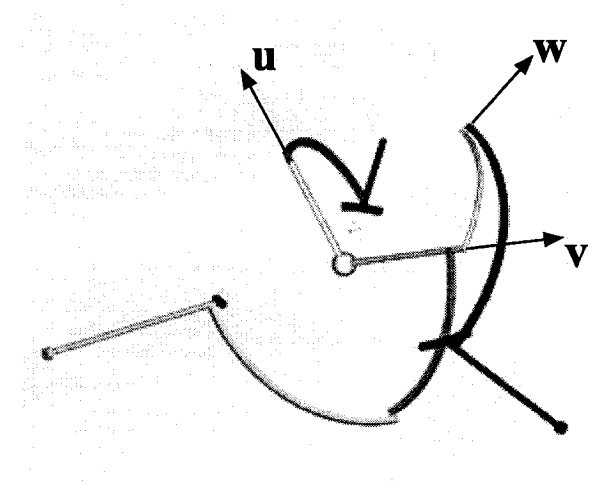


FIGURE 4.5. Spherical Stephenson mechanism with a streamlined coupler link

Figure 4.6 shows the mirror image of the mechanism of Fig. 4.5; the reflected mechanism was obtained as the mirror image of the given one with respect to the plane passing through the centre of the mechanism and parallel to the unit vectors \mathbf{u} and \mathbf{v} . The images of \mathbf{u} , \mathbf{v} and \mathbf{w} are \mathbf{u}' , \mathbf{v}' and \mathbf{w}' , respectively.

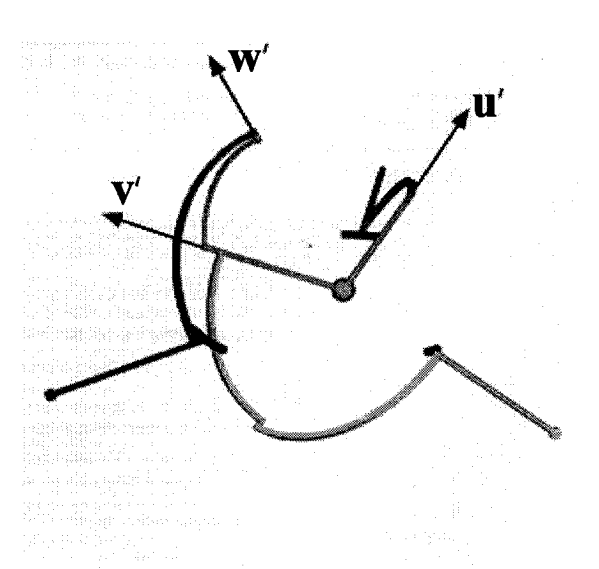


FIGURE 4.6. Mirror image of the optimum spherical Stephenson mechanism

Figure 4.7 shows the layout of the four mechanisms assembled.

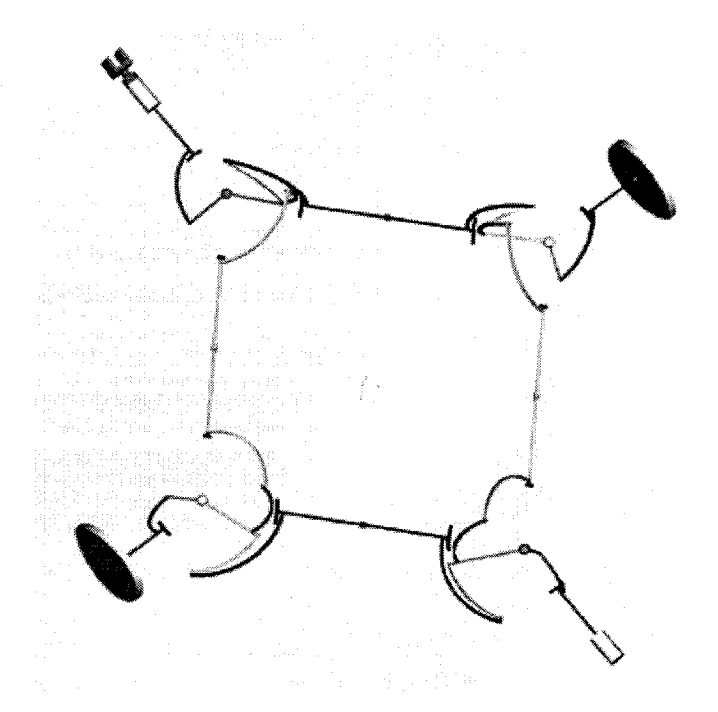


FIGURE 4.7. The four Stephenson mechanisms upon assembly

Figure 4.8 shows the final embodiment, in which the coupler link was designed based on the standard cross of a commercial universal joint, and the input link was shaped as a yoke, as displayed in Fig. 4.9.

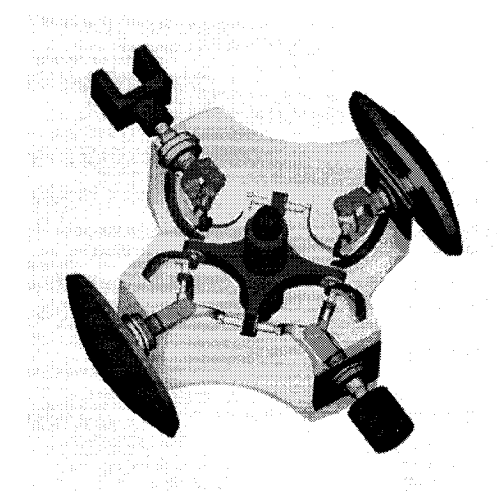


FIGURE 4.8. Final embodiment of the solution mechanism

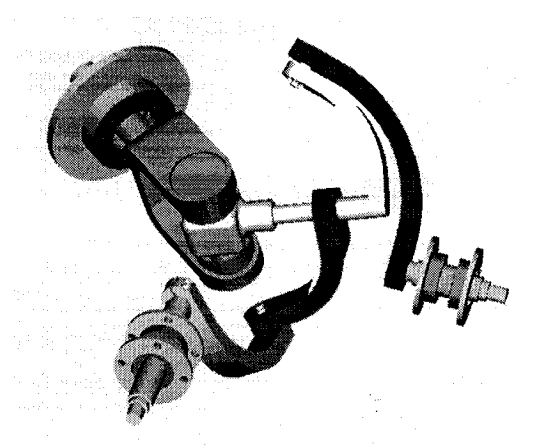


FIGURE 4.9. Embodiment of the spherical Stephenson mechanism

More specifically, the coupler link was designed using the cross element of an off-the-shelf universal joint, namely, the 302-0400 cross and bearing of G & G Manufacturing Co. of Omaha, Nebraska, to which a link on its end was added, along with two housing-bearing caps, as shown in Fig. 4.10. We selected needle bearings, of SKF RNAO $12 \times 22 \times 12$ TN. The coupler will be assembled to the yoke by press-fitting.

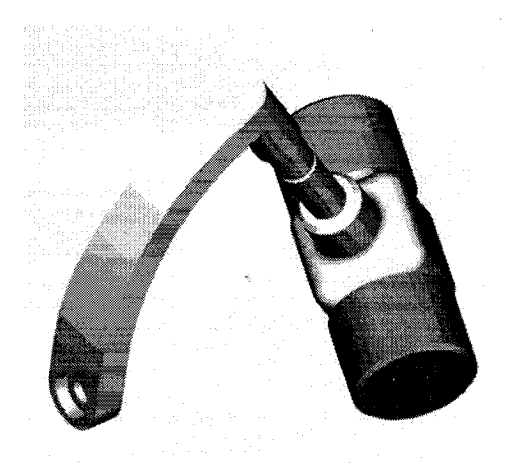


FIGURE 4.10. The shaping of the coupler link

Below we outline the design of the structure supporting the chain of Stephenson mechanisms.

4.4. The Design of the Mechanism Mounting

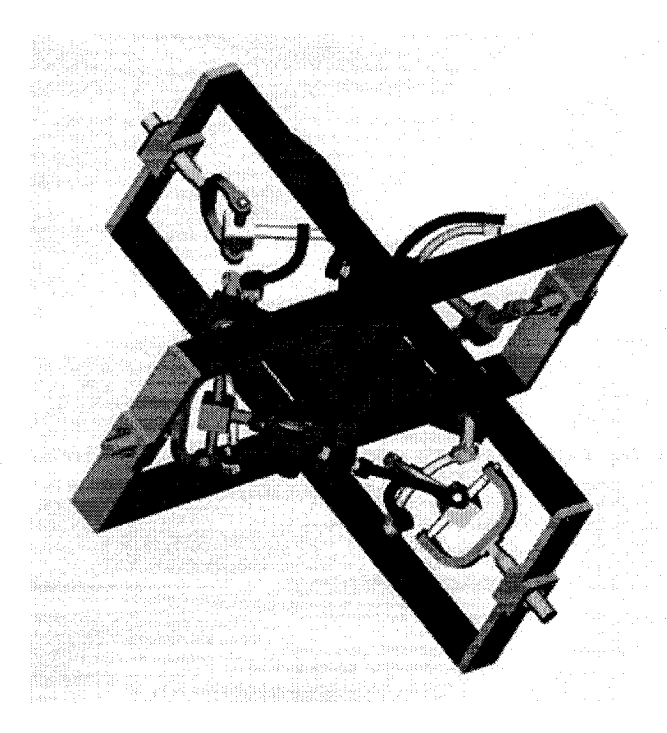


FIGURE 4.11. Preliminary concept of the structure that will support the four Stephenson mechanisms

Figure 4.11 shows a preliminary conceptual design for the structure supporting the four Stephenson mechanisms upon assembly. This structure is built upon two X-shaped elements, called the X-elements, each made up of two identical beams intersecting each other at the midpoints of their axes. Each element, moreover, has a cylindrical bore of axis normal to the common midplane of the pair of beams. The bore is needed to lodge the bearings that support the central element carrying the four output shafts of the Stephenson mechanisms. We can anticipate a high stress concentration occurring on the sharp corners of the X-elements, as predicted by the theory of elasticity (Neuber 1961; Timoshenko and Woinowsky-Krieger, 1959). Additionally, this structure needs four beams joining the X-elements, with a reduced contact area to allow for a robust assembly; not only this, the preliminary concept of Fig. 4.11 is unpleasant to the eye. In order to improve the design, we decided to first round the corners of the X-element, to produce a low change in curvature, that

would reduce the stress concentration, while providing for a flat surface on the sides of the structure to receive the input-shaft bearings of the Stephenson mechanisms. To this end, we can design the structure using conventional circular rounding in the corners; however, since the blending of a circular arc with a line along a tangent of the arc is continuous to the first order only (C^1 -continuity), we will have stress concentration due to the curvature discontinuity at the points of the edges where the circular rounding and the flat surface blend (Neuber 1961). Hence, we resort to Lamé curves, that are C^2 -continuous. These curves were discovered by the French mathematician Gabriel Lamé in the 1800's and later used by the Danish inventor Piet Heins, who called them superellipses (Gardiner, 1965). Lamé curves lie between the ellipse and the rectangle. Just to mention one pertinent design application, the Lamé curves or superellipses were used in the design of the Olympic Stadium in Mexico City. The Lamé curves are recalled below.

The canonical form of the equation of the ellipse is,

$$\left(\frac{x}{a}\right)^2 + \left(\frac{y}{b}\right)^2 = 1\tag{4.1}$$

Changing the exponents of eq.(4.1) to a more generic value p, we obtain the equations of the Lamé curves, namely,

$$\left|\frac{x}{a}\right|^p + \left|\frac{y}{b}\right|^p = 1\tag{4.2}$$

in which increasing the integer exponent p, the curve looks more and more like a rectangle. In the limit, as $p \to \infty$, the Lamé curve becomes a rectangle.

Lamé curves for $p=1,\ 2,\ 3,\ 4,\ 5$ and 6 are shown Fig. 4.12 for a=200 and b=100.

Figure 4.13 shows the curvature distribution κ for each of the foregoing Lamé curves, plotted in the interval [-200, 0]. From the same figure, we can see that the plots start from a value close to zero, to end with a value close to zero as well, that

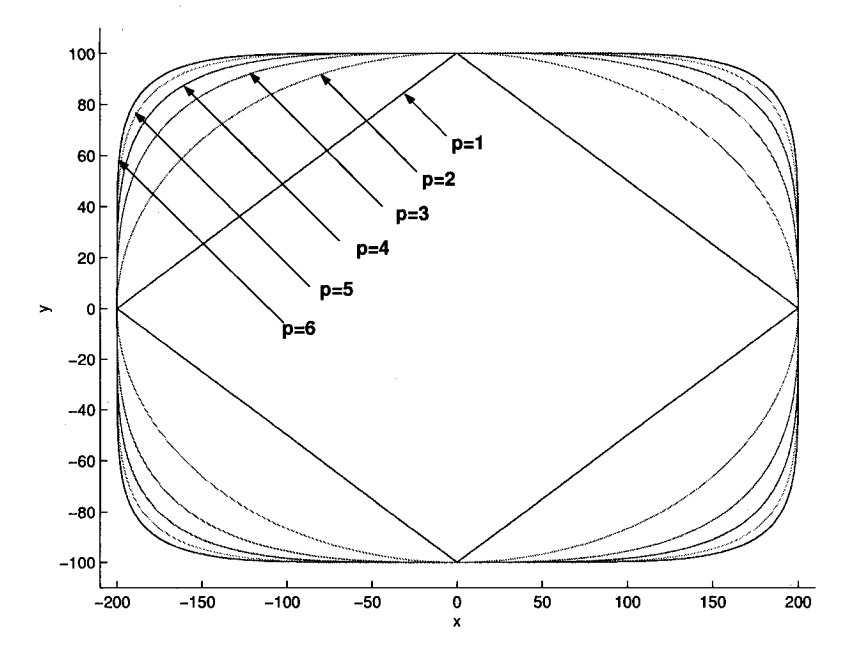


FIGURE 4.12. Lamé curves for p = 1, 2, 3, 4, 5 and 6

corresponds to the flat regions of the Lamé curves. The curve that has the highest change in curvature is that for which p=6.

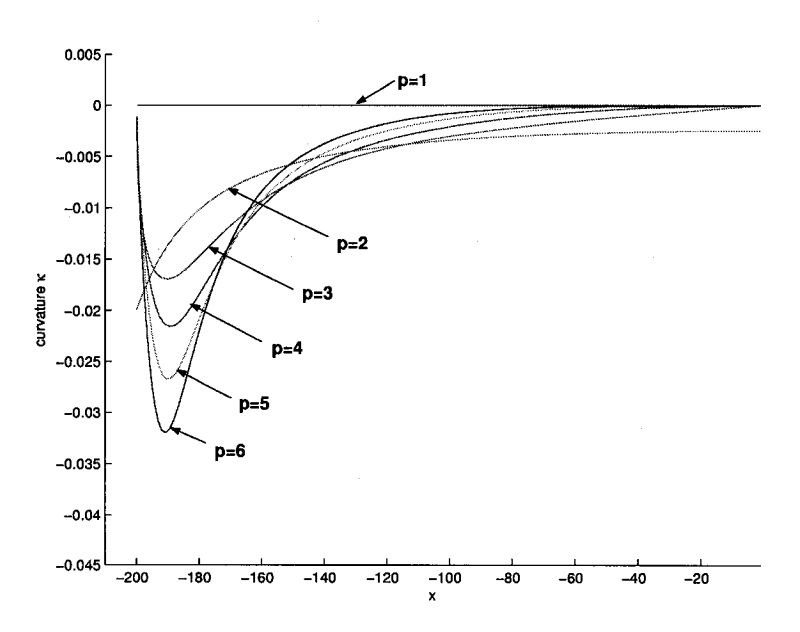


FIGURE 4.13. Curvature κ vs. x for Lamé curves with exponents $p=1,\ 2,\ 3,\ 4,\ 5$ and 6

To design the structure, that we call the *cover*, we select the Lamé curve for p=4 for its inside surface, which gives us a reasonable change in curvature. For the outside surface we select the Lamé curve for p=6 that gives a pleasing appearance.

Now, the structure must enclose the chain of Stephenson linkages to support them, but the structure must allow the assembly of the whole mechanism. Hence, a structure made of one single part is out of the question. Apparently, the preliminary design of Fig. 4.11 is composed of six parts, the two cross elements and the four beams joining them. We should aim at a simpler design, i.e., one with fewer parts. We decided to use four parts: two identical parts formed by (i) cutting the whole structure into two identical halves and (ii) removing rectangular portions from each half, which would be used to join the two halves upon assembly of the mechanism, thereby ending up with a total of four parts for the structure.

Figure 4.14 shows the side view of the cover.

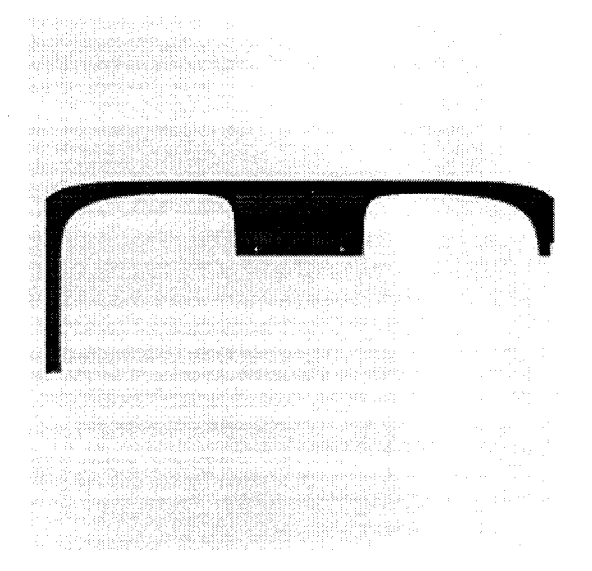


FIGURE 4.14. Side view of the designed cover based on Lamé curves

The assembly of the four parts of the structure, with the Stephenson mechanisms removed, is shown in Fig. 4.15.

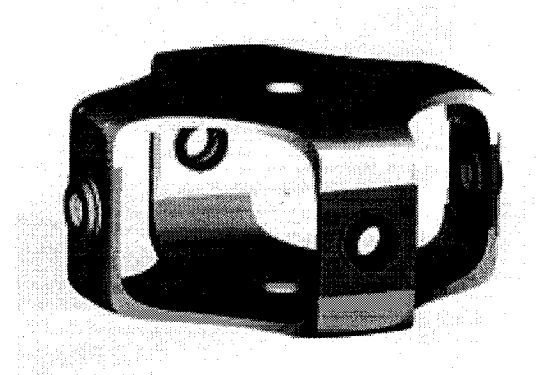


FIGURE 4.15. The assembly of the cover

The assembly of the Stephenson mechanisms with their supporting structure, the cover, the two conjugate spherical cams, the gripper and the counterweight are displayed in Fig. 4.16.

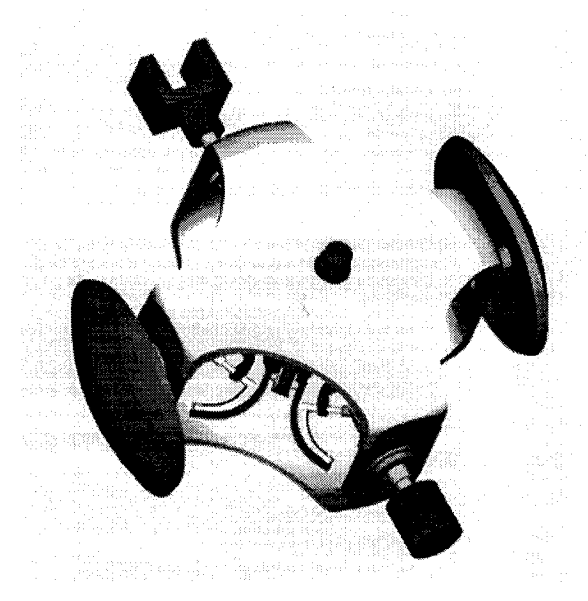


FIGURE 4.16. Final embodiment with the design of the cover

The assembly of the final embodiment of the pitch-roll wrist that comprises the two cams, the gripper, the counterweight and the roller-carrying disks is illustrated

4.4. THE DESIGN OF THE MECHANISM MOUNTING

in Fig. 4.17. The two-dof pitch-roll wrist is to be actuated by two face-to-face motors driving the two shafts mounted on the two supporting brackets.

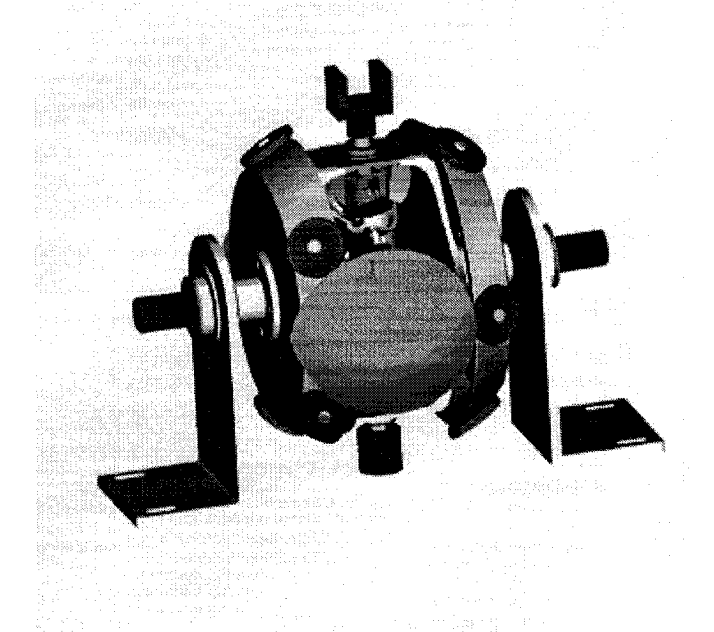


FIGURE 4.17. Embodiment of the complete pitch-roll wrist

Concluding Remarks

5.1. Conclusions

The optimum design of a spherical epicyclic transmission based on the concept of Speed-o-Cam reducers is the major subject of this thesis. This transmission is intended to compete with its current counterpart based on bevel gears, and used to produce the pitch and roll motions of a robotic gripper, what is called a pitch-roll wrist. A previous design of the epicyclic transmission comprises three pairs of conjugate-cam subassemblies that are virtually impossible to machine out of a single blank, as needed for maximum accuracy. An alternative transmission, based on spherical Stephenson mechanisms, was developed, as reported here, to replace the previous design. The new transmission comprises two pairs of spherical Stephenson mechanisms; one of each pair, is the main mechanism, the other its mirror image. The assembled layout was explained in Chapter 1. Out of the two distinct spherical mechanisms, we designed only one; the second was designed as the mirror image of the main mechanism.

In order to improve the machining accuracy of the spherical cams, we introduced in Chapter 2 a convexity condition that leads to a convex cam.

We described the design procedure of the spherical Stephenson mechanism in Chapter 3. We proceeded by first deriving the synthesis equations of the four and fivebar loops of the Stephenson mechanism using Wampler's rotation-matrix formulation. Then, we worked with the optimization of the four-bar loop using its loop equation and the zero-mean condition to find the link dimensions that lead to a drag-link mechanism with optimum transmission quality. The optimum mechanism has a transmission angle with a symmetric distribution throughout a full rotation of the input link. By dyalitic elimination, using the four and five-bar loop equations, we derived a single equation involving the input and the two output angles of the Stephenson mechanism. Taking into account the input-output pairs of the four-bar loop and the single equation of the whole mechanism, we prescribed a set of 360 input-output triads to be met with the synthesis equations. These were met approximately by means of least-square optimization, to obtain the link dimensions of the optimum mechanism. The results of the optimization were validated with a PRO/ENGINEER virtual prototype, as reported in Chapter 4.

5.2. Recommendations for Future Research

Future work expanding that reported here should include:

- (i) A dynamical analysis of the mechanism.
- (ii) The design of an inertially isotropic coupler of the spherical Stephenson mechanism, in order to avoid shaking forces and moments on the device.
- (iii) A suitable geometric modeling of spherical mechanisms, as explained below. PRO/ENGINEER is a CAD software that was not intended to model spherical mechanisms, which are overconstrained versions of their spatial counterparts. The rounding error produced during the assembly of links whose dimensions and locations are not defined by integer values is a cause of major alignment problems. The default assembly-tolerance in PRO/ENGINEER does not allow for too much error. Generally, the problems of alignment

5.2. RECOMMENDATIONS FOR FUTURE RESEARCH

start with the last links to assembly. In order to help the joint axes of those links intersect at the centre of the mechanism, it is necessary to play with the number of decimals and rounding-off of the numerical values of the last links to assembly. The number of those decimals that we chose was four.

(iv) A design of the spherical linkages robust against manufacturing errors, possibly replacing some revolutes by cylindrical joints.

Last, but no means least, the designer should recognize the practical aspect of designing spherical mechanisms. Manufacturing and assembly errors are bound to make it extremely difficult to actually produce a highly overconstrained mechanism. How to design robustly such mechanisms at an affordable cost is a challenging research task that should be undertaken in the future.

REFERENCES

Angeles, J., 1982, Spatial Kinematic Chains. Analysis, Synthesis, Optimization, Springer-Verlag, Berlin.

ANGELES, J., 2003, *Kinematic synthesis*, Lecture notes, Department of Mechanical Engineering, McGill University, Montreal, Quebec, Canada.

Angeles, J. and Bernier, A., 1987, "The global least-square optimization of function-generating linkages", ASME J. of Mechanisms, Transmissions, and Auto. in Design, Vol. 109, No. 2, pp. 204–209.

Angeles, J. and López-Cajún, C.S., 1991, Optimization of Cam Mechanisms, Kluwer Academic Publishers, Dordrecht.

BIDAULT, F., ANGELES, J. AND TENG, C-P., 2001, "Structural optimization of the links of a parallel spherical manipulator", Technical Report TR-CIM-01-05, Centre for Intelligent Machines, McGill University.

Chiang C.H., 1998, *Kinematics of Spherical Mechanisms*, Cambridge University Press, Cambridge, U.K.

COHEN, R., LIPTON, M.G., DAI, M.Q. AND BENHABIB B., 1992, "Conceptual design of a modular robot", ASME J. of Mechanical Design, Vol. 114, pp. 117–125.

Gardiner, M., 1965, "The superellipse: a curve that lies between the ellipse and the rectangle", Sci. Am., Vol. 21, pp. 222–234.

GE, Q. J. AND LAROCHELLE, P. M., 1999, "Algebraic motion approximation with NURBS motions and its application to spherical mechanism synthesis", ASME J. of Mechanical Design, Vol. 121, No.12, pp. 529–532.

GE, Q. J., AND McCarthy, J. M., 1991, "The algebraic classification of the image curves of spherical four-bar motion", ASME J. of Mechanical Design, Vol. 113, No. 3, pp. 227–231.

González-Palacios, M.A. and Angeles, J., 1993, *Cam Synthesis*, Kluwer Academic Publishers, Dordrecht.

González-Palacios, M.A. and Angeles, J., 1999, "The design of a novel mechanical transmission for speed reduction", ASME J. of Mechanical Design, Vol. 121, No.4, pp. 538–543.

Gosselin, C., and Angeles, J., 1989, "Optimization of planar and spherical function generators as minimum-defect linkages", Mech. Mach. Theory, Vol. 24, No.4, pp. 293–307.

Gosselin, C.J. and Cloutier L., 1993, "The generating space for parabolic motion error spiral bevel gears cut by Gleason method", ASME J. of Mechanical Design, Vol. 115, pp. 483–489.

Gosselin, C., and Hamel J.F., 1994, "The agile eye: a high-performance three-degree-of-freedom camera-orienting device", Proc. IEEE, International Conference on Robotics and Automation, San Diego, May 8–13, Vol.1, pp. 781–786.

Ghuneim, T., 2003, "Design of a pitch-roll mechanism using spherical cam-roller pairs", Technical Report, Department of Mechanical Engineering & Centre for Intelligent Machines, McGill University, Montreal, Canada.

Ghuneim, T., Angeles, J., and Bai, S., 2004, "The design of a novel pitch-roll wrist with spherical cam-roller pairs", to appear in Proc. 9th International Symposium on Advances in Robot Kinematics, Sestri Levante, Italy, June 28 - July 1.

Hartenberg, R.S. and Denavit, J., 1964, *Kinematic Synthesis of Linkages*, McGraw-Hill Book Company, New York.

Hervé, J.M., 1978, "Analyze Structurelle des Mécanismes par Groupes de Déplacements", Mech. Mach. Theory, Vol 13, pp. 437–450.

HOWARD, R. D., 2002, "Design of a robotic wrist and tool-exchange mechanism for satellite servicing", Proc. 36th Aerospace Mechanism Symposium, NASA Glenn Research Center.

JENSEN, P.W., 1987, Cam Design and Manufacture, Marcel Dekker, Inc., New York.

Kohli, D., and Khonji, A., 1994, "Grashof-type rotatability criteria of spherical five-bar linkages", ASME J. of Mechanical Design, Vol. 116, pp. 99–104.

LEE, M.K., 2001, Design for Manufacturability of Speed-Reduction Cam Mechanisms, M.Eng. Thesis, Dept. of Mechanical Engineering, McGill University, Montreal.

Liu, Z., and Angeles, J., 1993, "Data-conditioning in the optimization of function-generating linkages", ASME Advances in Design Automation, DE-Vol. 65-1, pp. 419–426.

MERLET, J-P., 1993, "Algebraic-geometry tools for the study of kinematics of parallel manipulators", in Angeles J., Hommel G. and Kovács P. (eds), Computational Kinematics, Kluwer Academic Publishers, pp. 183–194.

NEUBER, H., 1961, Theory of Notch Stresses: Principles for Exact Calculation of Strength with Reference to Structural Form and Material, Springer-Verlag, Berlin.

NORTON, R.L., 2001, Design of Machinery, Second Edition, McGraw-Hill, Book Co., New York.

PRIMROSE, E., FREUDENSTEIN, F., AND ROTH, B., 1967, "Six-bar motion, II. The Stepenson-1 and Stephenson-2 mechanism", Archive for Rational Mechanics and Analysis, Vol. 24, pp. 42–72.

RAUCHFUSS, J.W. AND YANG, D.C.H., 2000, "A geometric approach for determining exact point accessibility of robotic manipulations", ASME J. of Mechanical Design, Vol. 122, pp. 287–293.

ROSHEIM, M.E, 1989, Robot Wrist Actuators, John Wiley & Sons, New York.

Salmon, G., 1885. Lessons Introductory to the Modern Higher Algebra. Chelsea Publishing Co., New York.

Teng, C.P., and Angeles, J., 2001, "A sequential-quadratic-programming algorithm using orthogonal decomposition with Gerschgorin stabilization", ASME J. of Mechanical Design, Vol. 123, pp. 501–509.

Tsai, L. W., 1988, "The Kinematics of Spatial Robotic Bevel-Gear Trains", IEEE, J. of Robotics and Automation, Vol. 4, No.2, pp. 150–156.

Wampler, C.W., 2004, "Displacement Analysis of Spherical Mechanisms Having Three or Fewer Loops", ASME J. of Mechanical Design, Vol. 126, No.1, pp. 93–100.

Wei, E-J., Lai, H-Y., Chen, C-K., 2000, "Machine tool setting for the manufacturing of spherical cams", J. of Materials Processing Technology, Vol. 100, pp. 147–155.

WIITALA, J.M., STANISIC, M.M., 2000, "Design of an Overconstrained and Dextrous Spherical Wrist", ASME J. of Mechanical Design, Vol. 122, pp. 347–353.

Yang, S-C., 2001, "Determination of spherical cam profiles by envelope theory", J. of Materials Processing Technology, Vol. 116, pp. 128–136.

YANG, D.C.H., LIN, E.Y. AND CHENG, S.Y., 1990, "Primary workspace of industrial robots with roll-pitch-yaw wrists", ASME J. of Mechanical Design, Vol. 112, No. 3, pp. 347–353.

Yang, D., and Rauchfuss, J., 2001, "A new zero-dimension robot wrist: Design and accessibility analysis", The International Journal of Robotics Research, Vol. 20 (2), pp. 163–173.

Zanganeh, K.E., and Angeles, J., 1994, "On the optimum design of planar and spherical drag-link mechanisms", ASME J. of Mechanism Synthesis and Analysis, DE-Vol. 70, No.4, pp.183–190.

Document Log:

SERGIO HERNANDEZ

Centre for Intelligent Machines, McGill University, 3480 University St., Montreal (Quebec) H3A 2A7, Canada, Tel.: (514) 398-4488

 $\textit{E-mail address} : {\tt sergiohn@cim.mcgill.ca}$

Typeset by $\mathcal{A}_{\mathcal{M}}\mathcal{S}\text{-}\mathbb{I}^{\underline{A}}T_{\underline{B}}X$